Bordbar, Hadi; Hyppänen, Timo

Line by line based band identification for non-gray gas modeling with a banded approach

Published in:
International Journal of Heat and Mass Transfer

DOI:
10.1016/j.ijheatmasstransfer.2018.06.093

Published: 01/12/2018

Document Version
Peer-reviewed accepted author manuscript, also known as Final accepted manuscript or Post-print

Line by line based band identification for non-gray gas modeling with a banded approach

Hadi Bordbar*[1,2], Timo Hyppänen[2]

[1] Department of Civil Engineering, School of Engineering,

Aalto University, Finland.

[2]Laboratory of Modelling of Energy Systems, School of Energy Systems,

The accepted version of the published paper of

Bordbar, H. & Hyppänen, T. 1 Dec 2018 In : INTERNATIONAL JOURNAL OF HEAT AND MASS TRANSFER. 127, p. 870-884 15 p.

Abstract

The banded approach or box model is a method to include the non-grayness of combustion gases in radiation heat transfer calculations. However, the determination of the correct limits for the bands and the effective band absorption coefficients is still something of a black art. In this study, the line by line (LBL) spectral absorption coefficient profile has been implemented to obtain the effective number of bands, and bands' limits for pure H_2O, pure CO_2 and a H_2O-CO_2 gas mixture. A mathematical technique has been used to smooth the LBL profiles of pure gases in atmospheric pressure in order to be used for identifying the gray bands. The optimization for selecting the bands is done by analyzing the radiative heat transfer in several one-dimensional benchmarks. After obtaining the optimal band dividing scheme, a set of correlations for the pressure based gray band absorption coefficient of pure gases is found by integrating the line by line spectral absorption coefficient weighted by the corresponding black body intensity along the bands. In contrary to the previous similar works, by using the LBL data for pressure based gray absorption coefficient of the bands, the current correlations are independent of gas concentration and path length. The present approach could successfully support the non-gray walls. The method has been validated using several benchmarks and exhibited comparable accuracy with other available models.

Keywords: Radiation heat transfer, Banded approach, Line by line spectral absorption coefficient, Non-gray gas modeling, Band absorption coefficient, Non-gray wall.

Highlights:

- A smoothing technique is used to analyze the LBL spectral profile.
- The optimal scheme for dividing the spectrum to the gray bands is determined.
- The current banded approach models the non-gray walls.
- LBL spectral profile is used to calculate the band absorption coefficient.
- Simple correlations for band absorption coefficients have been obtained.

Nomenclature

$b_{i,j}$	coefficients of polynomial correlation (eq. 28)
C	linear scattering phase function coefficient (-)
$E_{b\lambda}$	spectral blackbody emission (W. m^{-2})
f	blackbody emissive fractional function
G	incident radiation (W. m^{-2})
I	radiation intensity (W· sr^{-1})
L	length of the benchmarks (m)
M	number of ordinates
N_b	number of bands
n	refractive index (-)
q	radiative heat flux (W. m^{-2})
RST	radiative source term (W. m^{-3})
r	position vector
S_G	additional source of incident radiation (W. m^{-2})
$\hat{s}$	solid angle (sr)
T	temperature (K)
W_i	The weight factor of each band (Equation 16)
w_m	the weight associated with each ordinate (μ_m)
Y	the spherical harmonics in formulation of P1 method

Greek letters

β	extinction coefficient (m^{-1})
γ_D, γ_L	Doppler and Lorentz line half width (cm^{-1}/atm)

ε_w	wall emittance (-)
η	wave number (cm^{-1})
μ_m	direction cosine
κ_P	Pressure based absorption coefficient ($atm^{-1}cm^{-1}$)
κ	absorption coefficient (m^{-1})
$\overline{\kappa}_i$	mixture linear absorption coefficient of the gray bands (m^{-1})
σ	Stefan–Boltzmann constant (5.67×10^{-8} W. m^{-2} K^{-4})
σ_S	scattering coefficient (m^{-1})
λ_1, λ_2	the wavelength of band limits (μm)
ω_x^m	the weighting factor
χ	molar fraction (-)

Subscripts

b	blackbody
e	east cell boundary in DO formulation
mix	mixture
p	nodal point
P	pressure-based
λ, η	spectral based
$\Delta\lambda$	band based
w	wall, and west cell boundary in DO formulation

Abbreviations

ADF	absorption distribution function method
CFD	computational fluid dynamics
DO	discrete ordinate method
FSCK	full spectrum correlated-K method
LBL	line by line calculation
NB	narrow band method
Oxy	oxygen fired combustion
RTE	radiative transfer equation
SLW	spectral line based weighted sum of gray gas method
WSGG	weighted sum of gray gases model

1. Introduction

Radiation heat transfer in molecular gases is among the most difficult phenomena to model. Compared to other heat transfer phenomena, for the CFD simulation of radiative heat transfer, discretization in solid angles is needed in addition to that in space [1]. However, the more challenging part is to include the complex changes in the radiative properties of molecular gases with the wave number. The absorption coefficient of gases rapidly changes with wave number. The temperature, pressure and composition of a gas mixture strongly affect the shape and strength of the absorption lines in the spectrum [1]. All of these facts make the non-gray gas radiative heat transfer modeling of combustion gases so challenging. The simplest way to perform this complex calculation is to assume a single average value for the absorption coefficients in the whole radiative heat transfer spectrum where the radiative heat transfer occurs [2]. This so-called gray gas model has received much attention and has been widely used in engineering calculations due to its simplicity and low computational cost [1]. However, in many cases, this assumption may cause considerable inaccuracies [3].

Within the part of electromagnetic wave spectrum where the radiation heat transfer occurs, the gas spectral absorption coefficient profile forms a histogram containing millions of absorption lines [4]. Considering the effect of all these lines in solving the spectral radiative transfer equation is computationally too expensive and practically infeasible [5], and thus much attention has been devoted in the last decades to develop numerical models that could feasibly take the variation of the spectral absorption coefficients of the gases into account. The most accurate prediction of the spectral radiative properties is obtained by the so-called line by line calculation (LBL) that implements spectroscopic databases containing a set of spectral line parameters required to calculate the spectral absorption coefficient for the specified spectral location [4]. Due to the high computational cost of LBL, its usage is limited to providing a benchmark for the evaluation of other methods and the data needed for their development [5]. The second most accurate model in the list is the statistical narrow band model, which is based on the fact that the gas absorption coefficients vary more with the wavenumber than other quantities, and therefore the actual absorption coefficient can be replaced by smoothed values averaged over narrow bands on the order of 25 cm^{-1} [1]. Narrow band models calculate the transmissivity through a gas layer with a certain thickness taking into account the spectral variation within the narrow band. Hence, for a specific path length, one can assume a mean absorption coefficient in the narrow band. The method was originally proposed by Goody [6], and the model parameters for combustion conditions have been reported by [7, 8]. In principle, the narrow band models can be as accurate as LBL [1, 5].

There are number of other band methods with less accuracy such as the exponential wide band model [9], but in recent years, the global models have attracted the most attention. Because in practical heat transfer calculations, the total radiative heat flux and radiative source terms are the only parameters of interest, the global models implement spectrally integrated radiative properties to directly calculate them [1]. The most famous models in this category are the weighted sum of gray gases model [4, 10, 11], the full spectrum correlated-K method (FSCK) [12, 13], the spectral line based weighted sum of gray gas method (SLW) [14, 15] and the absorption distribution function method (ADF) [16]. Although the global models show promising accuracy, especially for homogenous single gases, implementing them in heterogeneous gas mixtures needs mixing schemes [17] or premixed absorption databases, which are usually obtained by LBL or NB calculations [18]. This means that implementing them in practical combustion systems needs a huge database and complex coding [13].

The main aim of this research is to provide a simple and accurate model to be easily implemented in commercial CFD solvers such as Ansys-Fluent to simulate non-gray gas radiation heat transfer in industrial-scale combustion equipment. Implementing the presented methodology needs

neither a deep understanding of all the details of gas spectral radiation heat transfer nor huge databases such as those used in NB [16], LBL [19], or FSCK [13].

The basis of the approach is the previously developed box model, which will be described in more detail. After reviewing the theory of solving the radiative transfer equation (RTE) in the box model by analyzing spectral absorption coefficient profiles obtained by LBL calculations, the suitable band limits for pure CO_2, pure H_2O and mixture of them will be presented. By using the LBL calculations, a database of pressure based gray band absorption coefficients with pre-obtained band limits will be compiled. Using optimization methods, a set of correlations for the pressure based gray band absorption coefficients will be presented and validated against several one-dimensional benchmarks. The emphasis would be on showing the unique capability of the present approach in supporting the non-gray walls. Considering the line by line results as the reference solution of the benchmarks, the predictions of the model have been compared with those of WSGG, FSCK models.

2. Theory

2.1. Spectral Discrete Ordinate Method for Slab Problem

The radiation heat transfer in one-dimensional parallel-plate enclosure containing participating gases have been widely used to develop and validate different non-gray gas models [5, 13, 20]. Here we use it to validate our selection of gray bands used in the present non-gray box model. DO method has been used to solve RTE for several non-gray models. Hence, here we briefly review the formulation of DO used in our analysis. Following [5, 21], the spectral radiation intensity at a nodal point (p) with a positive direction cosine (μ_m) for an emitting, absorbing but not scattering medium is given by

$$I^m_{\eta,p} = \frac{(\mu_m / \omega^m_x) I^m_{\eta,w} + \kappa_\eta I_{b\eta,p} \Delta x}{\mu_m / \omega^m_x + \kappa_\eta \Delta x} \tag{1}$$

in which $I^m_{\eta,w}$ is the upstream spectral radiation intensity along the discrete direction m, ω^m_x is the weighting factor relating the radiation intensity at nodal point to the upstream and downstream values (i.e. $I^m_{\eta,w}$ and $I^m_{\eta,e}$ for positive μ_m, respectively) and is given by

$$I^m_{v,p} = \omega^m_x I^m_{\eta,e} + (1-\omega^m_x) I^m_{\eta,w} \tag{2}$$

Following the hybrid scheme proposed by Liu et al. [21], the weighting factor (ω^m_x) is given by $\omega^m_x = \max(0.5, \omega^{m'}_x)$ where $\omega^{m'}_x = 1 - \alpha/\kappa_\eta$ and $\alpha = \mu_m / \Delta x$. The same formulation can be obtained for the directions with negative cosines.

The boundary condition in each wall is defined as [1]

$$I^m_{\eta,x=0} = I_{b1,\eta} - \frac{1-\varepsilon_{w1,\eta}}{\varepsilon_{w1,\eta}\,\pi} q_{1,\eta} \quad where \quad \mu_m > 0 \tag{3}$$

$$I^{m}_{\eta,x=L} = I_{b2,\eta} + \frac{1-\varepsilon_{w2,\eta}}{\varepsilon_{w2,\eta}\,\pi} q_{2,\eta} \quad where \;\; \mu_m < 0 \tag{4}$$

$q_{1,\eta}$ and $q_{2,\eta}$ represent the spectral radiative heat flux at the two surfaces and are given by

$$q_{1,\eta} = \varepsilon_{w1,\eta}(E_{b1,\eta} + \sum_{m=1,\mu_m<0}^{M} w_m \mu_m I^{m}_{\eta,x=0}) \tag{5}$$

$$q_{2,\eta} = -\varepsilon_{w2,\eta}(E_{b2,\eta} - \sum_{m=1,\mu_m>0}^{M} w_m \mu_m I^{m}_{\eta,x=L}) \tag{6}$$

Where M and w_m are the number of ordinates and the weight associated with each ordinate (μ_m), respectively. For all the cases, S8 discretization scheme is used and the values of ordinates and their weights are taken from Table 17.2 of [1].

For the black walls, the second term of the right hand side of equations (3) and (4) are eliminated and the solution is not iterative. However, for the cases with gray and non-gray walls, the iterative solution is needed and following [21], the iterative solution stops when

$$\max\left(\frac{G^{N}_{\eta,p} - G^{N-1}_{\eta,p}}{G^{N}_{\eta,p}}\right) \le 10^{-4} \tag{7}$$

Where N is the iteration number and $G^{N}_{\eta,p}$ is the spectral radiation incident calculated by

$$G^{N}_{\eta,p} = \sum_{m=1}^{M} w_m I^{m}_{\eta,p} \tag{8}$$

Implementing the spectral absorption profiles obtained by LBL calculations, we have obtained the reference solution of our one dimensional benchmarks to be used for assessment of other non-gray methods. After obtaining the radiative intensity field, the spectral radiative heat flux at the cell boundaries is obtained by [5]

$$q_{\eta}(x) = \sum_{m=1}^{M} \mu^m I^{m}_{\eta,x} w^m \tag{9}$$

The total radiative heat flux is then calculated by $q(x) = \int_{\eta} q_{\eta}(x) d\eta$ – and the radiative source term at the nodal points is calculated by

$$\left(-\frac{dq}{dx}\right)_p = -\frac{q_{e_p} - q_{w_p}}{x_{e_p} - x_{w_p}} \tag{10}$$

2.2. Formulation of DO for a General Non-Gray Solution

In addition to the present banded approach, two other global models have been included in this research; WSGG with two sets of coefficients reported by Bordbar et al. [4] and Smith et al. [11], and FSCK implementing the look up table recently reported by Wang et al. [13]. In general, the non-gray models offer the opportunity to solve the RTE only for a limited number which make them computationally feasible to be used in modeling of the practical combustion systems. For each time of solving RTE, they provide some values for absorption coefficient (such as k-values in FSCK, or gray gas absorption coefficients in WSGG) and the weighting factor corresponded to it (such as the non-gray stretching function (a-function) in FSCK or weighting factors in WSGG). The total results are then obtained by making summation over all the solutions of RTE by considering their weighting factors.

Hence, if for a general non-gray model, N_b is the number of times RTE should be solved, $\bar{\kappa}_i$ and $W_i, (i = 1...N_b)$ are the absorption coefficient and weighting factor of each time. The boundary condition is now written as

$$I^m_{i,x=0} = W_i \frac{\sigma T_1^4}{\pi} - \frac{1-\varepsilon_{w1,\eta}}{\varepsilon_{w1,\eta}\,\pi} q_{1,i} \quad where \quad \mu_m > 0 \tag{11}$$

$$I^m_{i,x=L} = W_i \frac{\sigma T_2^4}{\pi} + \frac{1-\varepsilon_{w2,i}}{\varepsilon_{w2,i}\,\pi} q_{2,i} \quad where \quad \mu_m < 0 \tag{12}$$

Where

$$q_{1,i} = \varepsilon_{w1,i}\left(W_i \frac{\sigma T_1^4}{\pi} + \sum_{m=1,\,\mu_m<0}^{M} w_m \mu_m I^m_{i,x=0}\right) \tag{13}$$

$$q_{2,i} = -\varepsilon_{w2,i}\left(W_i \frac{\sigma T_2^4}{\pi} - \sum_{m=1,\,\mu_m>0}^{M} w_m \mu_m I^m_{\eta,x=L}\right) \tag{14}$$

Once the intensity field is obtained, the radiative heat flux is calculated by $q_i(x) = \sum_{m=1}^{M} \mu^m I^m_{i,x} w^m$ and total radiative heat flux is then given by $q(x) = \sum_{i=1}^{N_b} q_i(x)$ and radiative source term is found as equation (10).

As the details of obtaining FSCK model parameters are out of scope of this research, we do not review them here. The details of FSCK have been well-documented by series of articles by Modest, see for instance [12, 13, 17, 20]. To obtain the corresponded values of k-value and the non-gray stretching function (a-function), the recently published look up table [13] has been used.

Theory and detailed description of WSGG are also well documented (see for instance [4, 11]) and are not repeated here. For this work, the values of gray gas absorption coefficients and their weighting factors have been taken from Bordbar et al. [4] and Smith et al. [11].

For the present banded approach, the pressure based gray band absorption coefficient of each band is calculated by

$$\bar{\kappa}_P\big|_{\eta_1-\eta_2} = \frac{\int_{\eta_1}^{\eta_2} \kappa_{P,\eta} I_{b,\eta} d\eta}{\int_{\eta_1}^{\eta_2} I_{b,\eta} d\eta} \tag{15}$$

Where η_1 and η_2 represent the wavenumber of the band limits. The obtained gray band absorption coefficients will be used to solve the RTE in each band. The weighting factor corresponded to each band is the blackbody emissive fractional function of the band as

$$W_i = f(n\lambda_2 T) - f(n\lambda_1 T) \tag{16}$$

Where λ_1 and λ_2 represent the wavelength of the band limits.

2.3. Formulation of P1 for a Banded Non-Gray Solution

DO has been used as the main RTE solver in the validation cases. It is because of the wider optical thickness range supported by DO, i.e. P1 is more suitable for optically thick regime. However, as the presented banded approach may be used by the readers in P1 method, the description of P1 banded solution is also briefly described in this section. The P1 approximation method and the discrete ordinate method (DO) are among the most popular RTE solvers used in engineering CFD calculations of participating media. P1 is the simplified form of a more general model of the PN approximation method or spherical harmonic method in which the radiative intensity is expanded into an orthogonal series of spherical harmonics [1] as

$$I_\lambda(r,\hat{s}) = \sum_{l=0}^{\infty} \sum_{m=-1}^{l} I_{\lambda,l}^m(r) Y_{\lambda,l}^m(\hat{s}) \tag{17}$$

where $I_{\lambda,l}^m(r)$ corresponds to the changes in the intensity with position, and $Y_{\lambda,l}^m(\hat{s})$ is the spherical harmonics that satisfy Laplace's equation in spherical coordinates. The details of the theory of the model are well documented in radiation heat transfer textbooks [1]. By using P1, the transfer equation for spectral incident radiation (G_λ) is given as

$$\nabla.(\Gamma_\lambda \nabla G_\lambda) - \kappa_\lambda G_\lambda + 4\kappa_\lambda n^2 E_{b\lambda} = S_{G\lambda} \tag{18}$$

where Γ_λ is defined as

$$\Gamma_\lambda = \frac{1}{3\beta_\lambda - C\sigma_{S\lambda}} \tag{19}$$

in which κ_λ, $\sigma_{S\lambda}$, β_λ and C represent the spectral absorption coefficient, spectral scattering coefficient, spectral extinction coefficient, and the linear scattering phase function coefficient, respectively. $S_{G\lambda}$ represents an additional source of incident radiation, if there is any.

For non-gray gas modeling with this banded approach, the incident radiation in each band is obtained by solving the following differential equation in each band ($i.e.\Delta\lambda$) using the gray band absorption coefficient obtained by LBL spectral absorption coefficient profiles.

$$\nabla.(\Gamma_{\Delta\lambda}\nabla G_{\Delta\lambda}) - \kappa_{\Delta\lambda} G_{\Delta\lambda} + 4\kappa_{\Delta\lambda} n^2 E_{b,\Delta\lambda} = S_{G\Delta\lambda} \tag{20}$$

Then, the spectral radiative heat flux is calculated as

$$q_{\Delta\lambda} = -\Gamma_{\Delta\lambda}\nabla G_{\Delta\lambda} \tag{21}$$

and its divergence or radiative source term in each band is obtained as

$$RST_{\Delta\lambda} = -\nabla q_{r,\Delta\lambda} = \kappa_{\Delta\lambda}\left(G_{\Delta\lambda} - 4n^2 E_{b,\Delta\lambda}\right) \tag{22}$$

in which $E_{b\Delta\lambda}$ is the spectral black body emission, which for each band is given as

$$E_{b,\Delta\lambda} = \left(f(n\lambda_2 T) - f(n\lambda_1 T)\right)\sigma T^4 \tag{23}$$

where $f(n\lambda T)$ is the fraction of the blackbody emissive power contained between 0 and $n\lambda T$, and λ_1 and λ_2 are the wavelength limits of the bands. The total radiative heat flux and radiative source term will be then obtained by performing a summation over all of the bands.

The other widely used RTE solver is the discrete ordinate method that solves the RTE for a finite number of discrete solid angles, each associated with a vector direction fixed in a coordinate system. The method can be used for obtaining the spectral radiative intensity in each band, and the total intensity is then calculated by performing a summation over all of the bands. The spectral incident radiation is then obtained by integrating the spectral radiation intensity over a 4π solid angle and the spectral radiative heat flux and radiative source term are calculated by equations 21-22.

By using the proposed banded approach, non-gray walls can also be modeled while the global models basically work only with gray or black walls. To provide such a possibility, the boundary conditions of the walls should be implemented in a banded base. For instance, the radiative heat flux leaving a non-gray wall in a specific band is given as

$$q_{out,\Delta\lambda} = \left(1-\varepsilon_{w,\Delta\lambda}\right)G_{\Delta\lambda} + \varepsilon_{w,\Delta\lambda} n^2 E_{bw,\Delta\lambda} \tag{24}$$

and the surface radiation incident on the selected spectral interval $\Delta\lambda$ is given as

$$G_{\Delta\lambda} = \Delta\lambda \int_{s.n>0} I_\lambda \, \hat{s}.\hat{n}\, d\lambda \tag{25}$$

3. Results and Discussions

3.1. Analysis of the LBL Absorption Spectrum

The detailed LBL pressure based absorption spectrum of two gas species of interest (CO_2 and H_2O) have been used to find the optimal band numbers, the bands' limits and the gray band absorption coefficient in each band. The theory and formulation used to generate such a detailed high resolution LBL absorption spectrum have been previously explained in many references, see for instance [4, 5]. In the present work, for all the analysis, a uniform spectral resolution of 0.02 cm^{-1} has been chosen for the wavenumber between 150 and 10000 cm^{-1}. The spectral resolution of 0.02 cm^{-1} has been reported as the optimal between accuracy and CPU cost as use of higher resolutions has a negligible influence on the results but significantly increase the computational time [5]. As the present method is aimed to provide a method for high temperature combustion system, the HITEMP2010 database [22] with the reference temperature of 296 K has been used as the spectral databases for LBL calculations. The spectral line profile to produce the histograms was chosen for each line based on the line characteristics obtained from the spectral database of HITEMP2010. In general, when Doppler half-width is comparable to the Lorentz half-width, then Voigt should be used. The criterion of γ_L/γ_D <10 has been considered for using the Voigt line profile otherwise Lorentz line profile has been used. A minimum limit of 10^{-9} cm^{-1} has been used for the line wings to be included (i.e. cut off limit).

In this research, the profile of the pressure based spectral absorption coefficient of CO_2 and H_2O in different temperatures in the range of our interest (300 K to 2400 K) has been analyzed. By this analysis, the grounds for selecting suitable band limits for the non-gray gas solution of the RTE with the present banded approach have been obtained. As Figure 1 shows, though the amount of the spectral absorption coefficient changes with temperature, the overall form of the curves along the spectrum are quite similar. Particularly, for all the profiles the extremums of the profiles are somehow located in certain wavenumber intervals. The same behavior can also be seen for H_2O spectral profile as shown in Figure 2.

The local data are quite noisy which means that there are a dramatic change in spectral absorption coefficient from one wave number to the next one and therefore it's challenging to find out which parts of spectrum include the most important absorption lines and hence should be taken into account in our non-gray modeling. We implemented a locally weighted scatter plot smoothing technique to smooth the spectral profiles to be used in identification of the gray bands. The smoothing is done by using the "*Smooth*" function of MATLAB R2017a with a quadratic polynomial for local regression. In this technique, each smoothed value is determined by neighboring data points defined within a specific span considering a regression weight function [23]. Using this technique, the high complex spectral data have been transferred to much smoother profiles in which we can identify the spectral location when a specific absorption coefficient occurs.

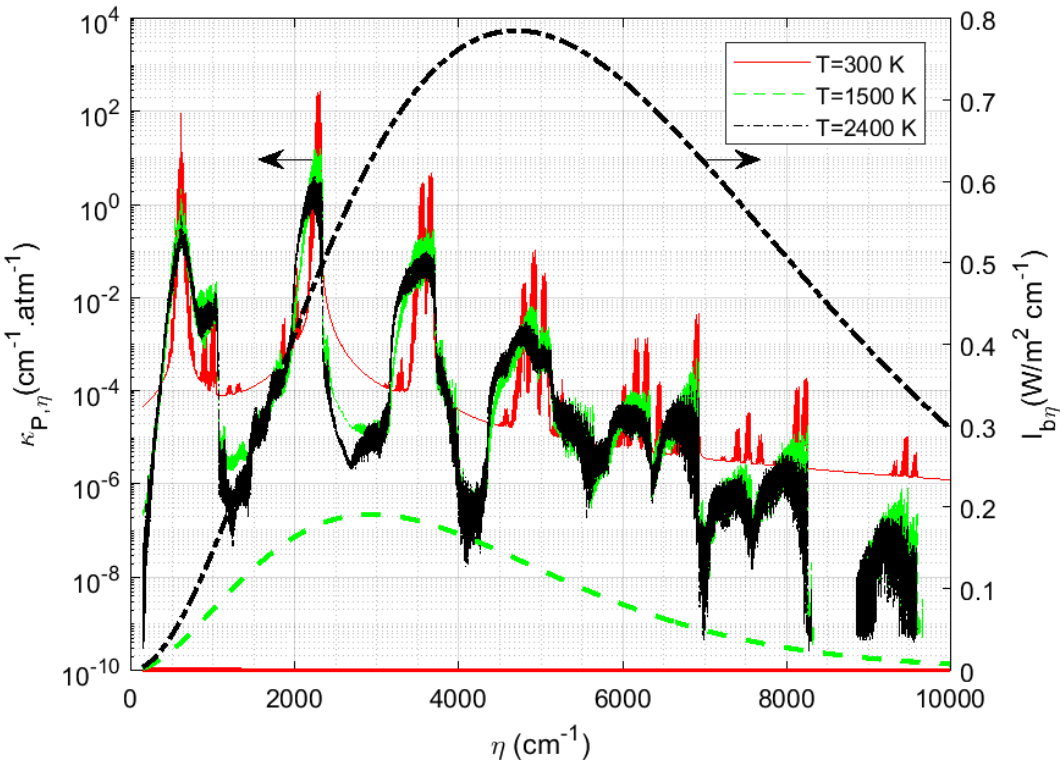

Figure 1. The pressure based spectral absorption coefficient of CO_2 at three different temperatures.

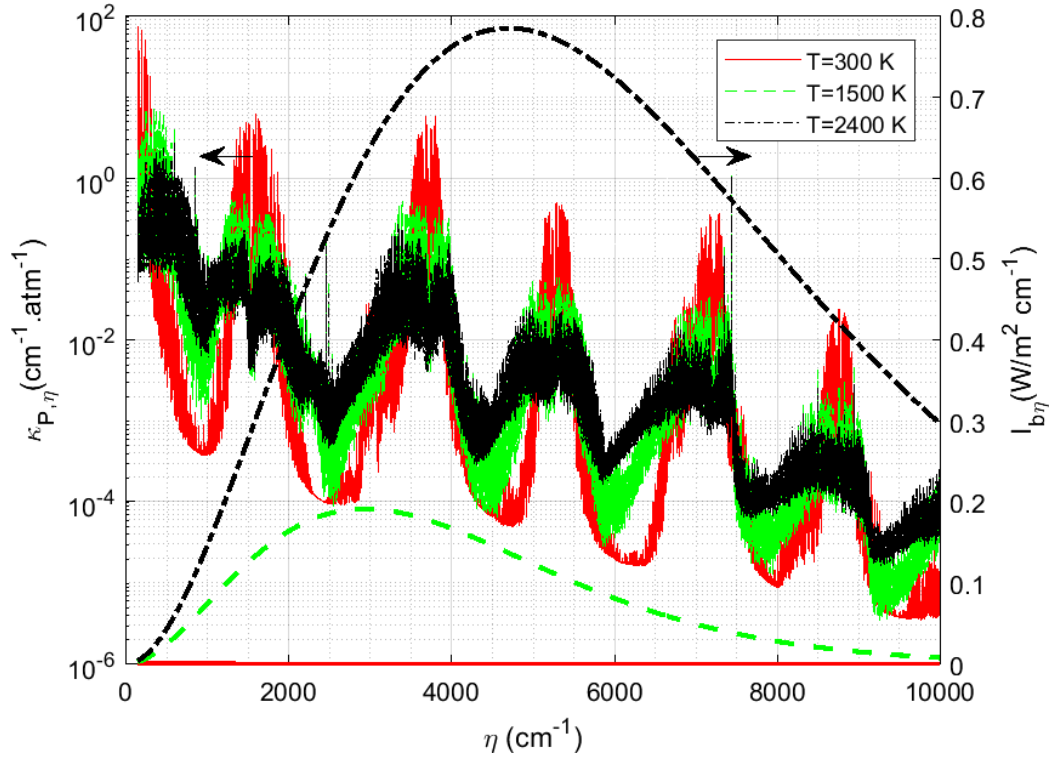

Figure 2. The pressure based spectral absorption coefficient of H_2O at three different temperatures.

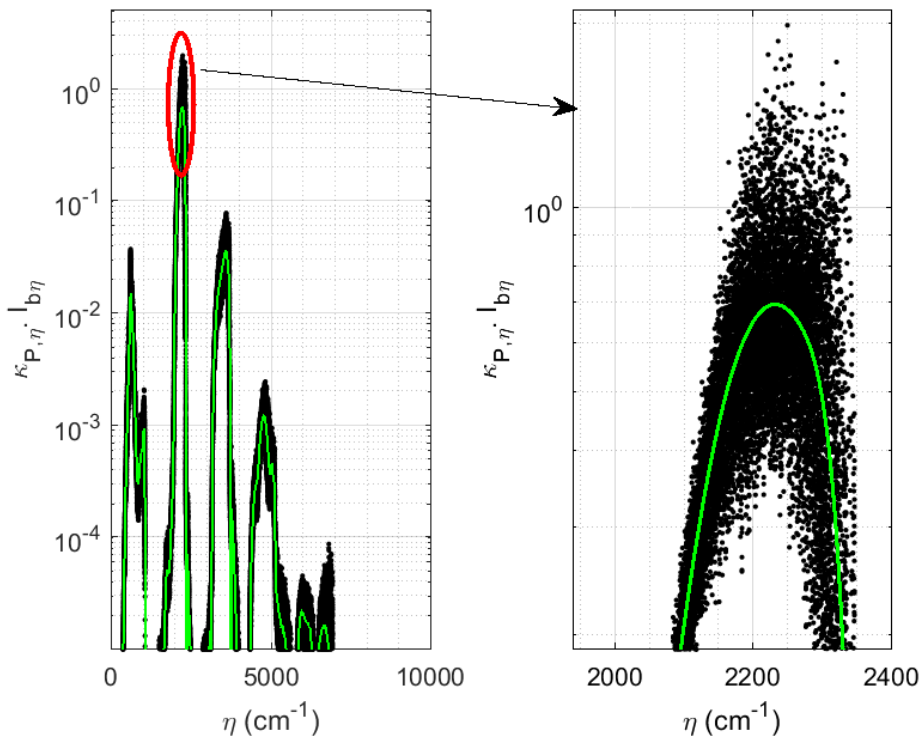

Figure 3. Smoothing the LBL based absorption spectrum of CO_2 at T=2400 K.

As equation (15) states, the pressure based gray band absorption coefficient is a function of both spectral pressure based absorption coefficient within the band and also the black body intensity which is used as the weight of integration. Therefore we determined the optimal band selection from the profile of $\kappa_{P,\eta} I_{b,\eta}$. As seen in Figures (1) and (2), the highest temperature in the range of our interest (2400 K) the widest and strongest absorption bands and therefore, if the optimal bands will be identified from spectral profile of 2400 K, the bands of other lower temperatures will be embedded inside the bands of 2400 K. Hence, we identify the optimal band selection for three different cases of pure CO_2, pure H_2O, and the case where both gases exist from the smoothed profiles of $\kappa_{P,\eta} I_{b,\eta}$ at 2400K. The span used for local averaging in smoothing function is 0.01. After obtaining the pressure based gray band absorption coefficient in each band, the mixture linear absorption coefficient is determined including the effect gas composition in the atmospheric gas mixture as

$$\bar{\kappa}_i = (\chi_{CO_2} \kappa_{P,i\_CO_2} + \chi_{H_2O} \kappa_{P,i\_H_2O}) \tag{26}$$

Where χ_{CO_2} and χ_{H_2O} are the mole fractions of CO_2 and H_2O, respectively. The similar equation but in a spectral form will be used when the LBL spectral absorption databases is used in DO for producing the benchmark solutions of one-dimensional test cases.

3.2. Band Selection for CO_2

As mentioned before, the base of the selecting the optimal gray bands in this research is the smoothed LBL based profile of $\kappa_{P,\eta} I_{b,\eta}$ at T=2400 K for three cases of pure H_2O, pure CO_2 and a mixture of these two gases. To select the optimal bands, we need to decide about the suitable

thresholds of $\kappa_{P,\eta}$ in which the spectral absorption coefficient can be integrated without losing too much accuracy. Beside, we need to decide the minimum values of $\kappa_{P,\eta}I_{b,\eta}$ below which the absorption is small enough to be ignored. The effect of lines with the smaller $\kappa_{P,\eta}I_{b,\eta}$ than these onsets can be safely ignored.

Case No.	$L(m)$	χ_{CO_2}	$T(K)$	Wall emittance
1	0.1	0.5	2000	1 (black wall)
2	0.1	0.5	2000	Eq. 27 (non-gray wall)
3	0.5	0.1	1500	1 (black wall)
4	0.5	0.1	1500	Eq. 27 (non-gray wall)

Table 1. Test cases of pure CO_2.

The selection of these limits of the smoothed $\kappa_{P,\eta}I_{b,\eta}$ and consequently the limits of the optimal gray bands for pure CO_2 is done through analysis of several one-dimensional benchmarks as listed in Table 1. The walls in all the benchmarks used in this work (Tables 1, 3, and 8) are kept at T_{wall}=300 K. To test the approach for non-gray wall, for some cases the wall emittance has been defined as

$$\varepsilon_{w,\eta}=\begin{cases}1 & 150\,cm^{-1}\le\eta\le 2509\,cm^{-1}\\ 0.5 & 2710\,cm^{-1}\le\eta\le 4230\,cm^{-1}\\ 0.1 & 4463\,cm^{-1}\le\eta\le 5639\,cm^{-1}\\ 0 & Other\ \eta\end{cases} \tag{27}$$

By testing several values as the onsets of $\kappa_{P,\eta}I_{b,\eta}$ profile, we have found out that for CO_2 the wave numbers with $\kappa_{P,\eta}I_{b,\eta}<1e^{-5}$ can safely be ignored without losing significant accuracy. To find suitable k-limits for dividing the spectrum into bands, we tested several values as the thresholds of $\kappa_{P,\eta}I_{b,\eta}$. Finer resolution means larger number of bands. For the sack of brevity, we introduce only two of the band dividing schemes examined for pure CO_2 benchmarks in Table 2. These two are schematically shown in Figure 4 with the thermal conditions of case 1 of Table 1.

Thresholds of $\kappa_{P,\eta}I_{b,\eta}$	Min. value of $\kappa_{P,\eta}I_{b,\eta}$	Number of bands
$1e^{-5}$-$1e^{-4}$, $1e^{-4}$-$1e^{-3}$, $1e^{-3}$-$1e^{-2}$, $1e^{-2}$-$1e^{-1}$, 0.1-1.0	$1e^{-5}$	25
$1e^{-3}$-$1e^{-1}$, 0.1-1.0	$1e^{-3}$	6

Table 2. Two forms of band selection examined for pure CO_2 benchmarks.

<u>25 bands' limits(cm^{-1}):</u> 413-462.5, 462.5-522.3, 522.3-597.5, 597.5-651.5, 651.5-748.5, 748.5-1072, 1072-1080, 1723-1954, 1954-2016, 2016-2082, 2082-2148, 2148-2344, 2344-2356, 2356-2359, 2359-2509, 3171-3222, 3222-3313, 3313-3564, 3564-3707, 3707-3731, 3731-3736, 3736-3879, 4463-4700, 4700-4963, 4963-5153.

<u>6 bands' limits (cm^{-1}):</u> 511.3-773.6, 1971-2066, 2066-2340, 2340-2361, 3196-3737, 4720-4857.

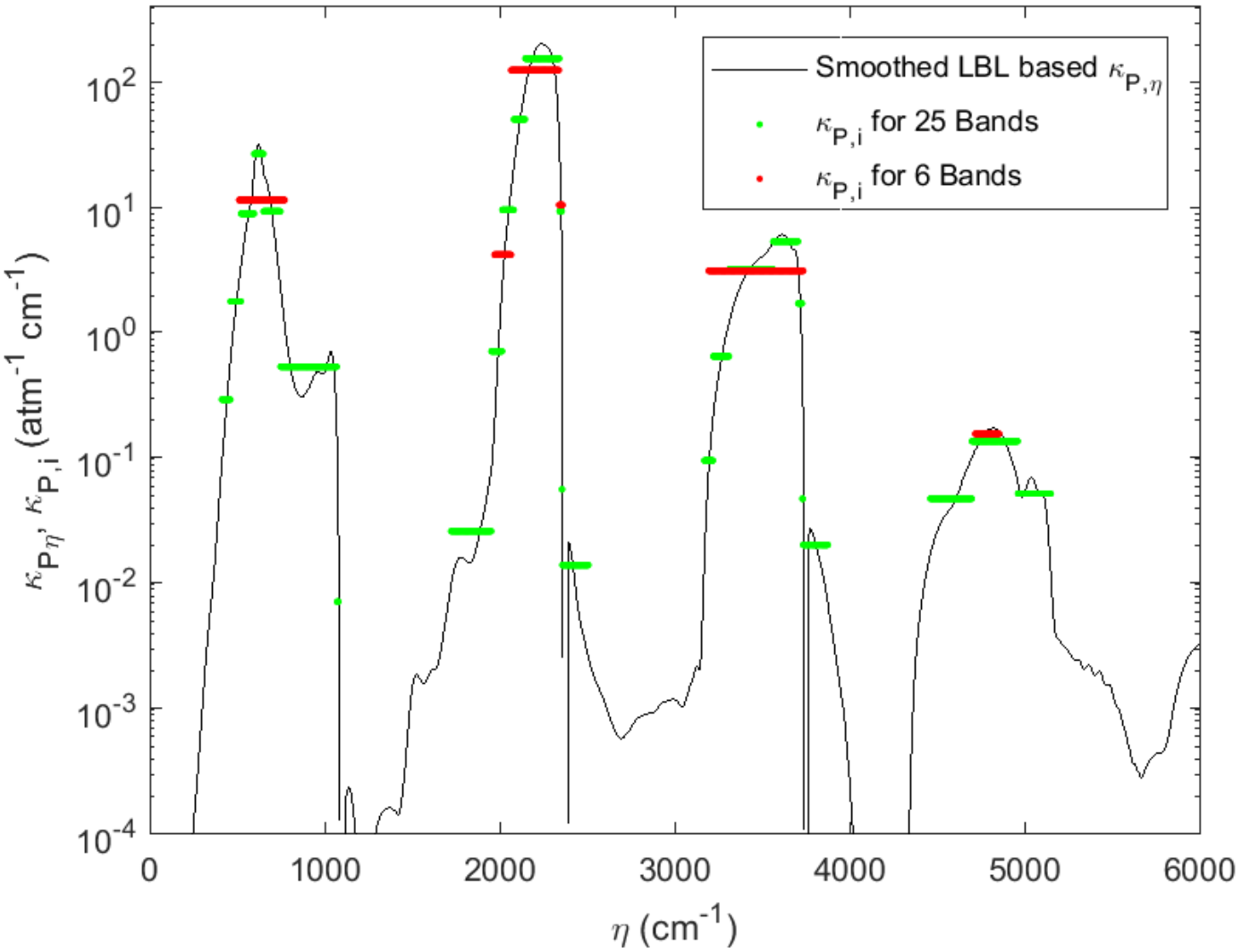

Figure 4. Illustration of how gray bands are identified for pure CO_2 from smoothed profile of the LBL spectral pressure based absorption coefficient. The figure shows the pressure based gray band absorption coefficient of Case 1 of Table 1.

The predictions of the present model have been compared with those of LBL high resolution absorption spectrum and those of other non-gray models, i.e. the WSGG with two sets of coefficients reported by Bordbar et al. [4] and Smith et al. [11] and the FSCK implementing the look up table for k and a-values [13]. Note that as the global models cannot support the non-gray walls, in cases with non-gray walls with the wall emittance profile defined by Eq. (27), an averaged value for wall emittance over entire spectrum, i.e. $\varepsilon_w = 0.3245$, have been used in calculations of WSGG and FSCKM.

Figures 5-8 show the radiative heat flux and radiative heat source along the slab for cases 1-4.

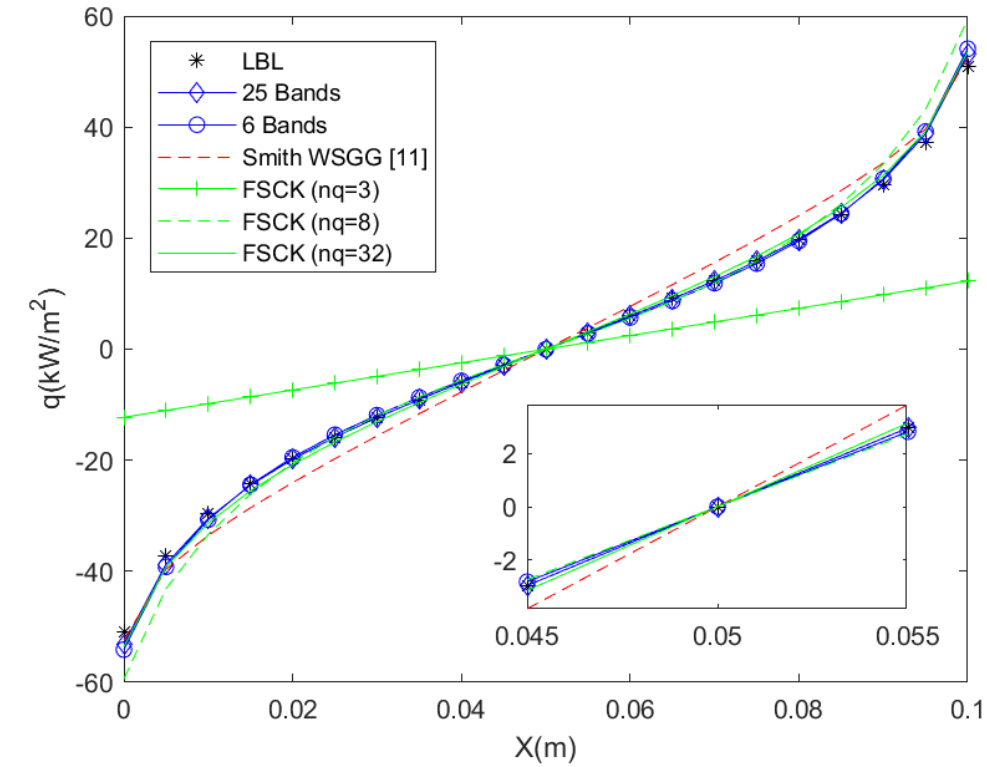

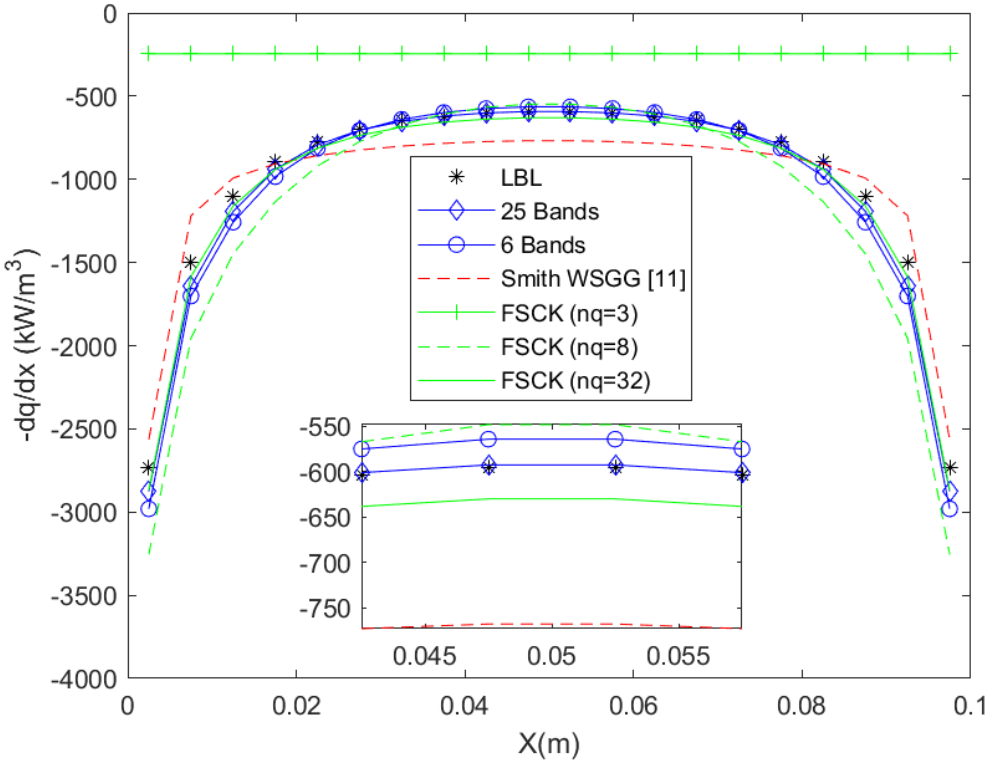

Figure 5. Radiative heat flux and radiative source along the slab for Case 1; CO_2; $\chi_{CO_2} = 0.5$, $L = 0.1\ m$, and $T = 2000K$ with black walls.

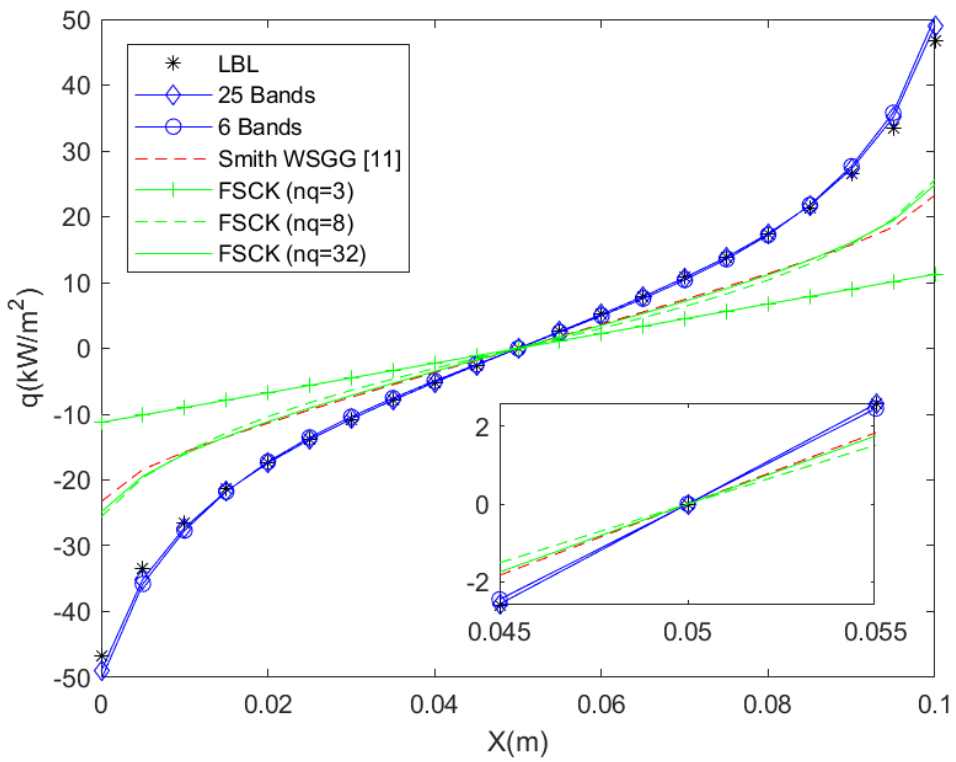

Figure 6. Radiative heat flux and radiative source along the slab for Case 2; CO_2; $\chi_{CO_2} = 0.5$, $L = 0.1\ m$, and $T = 2000K$ with non-gray walls as defined by Eq. (27).

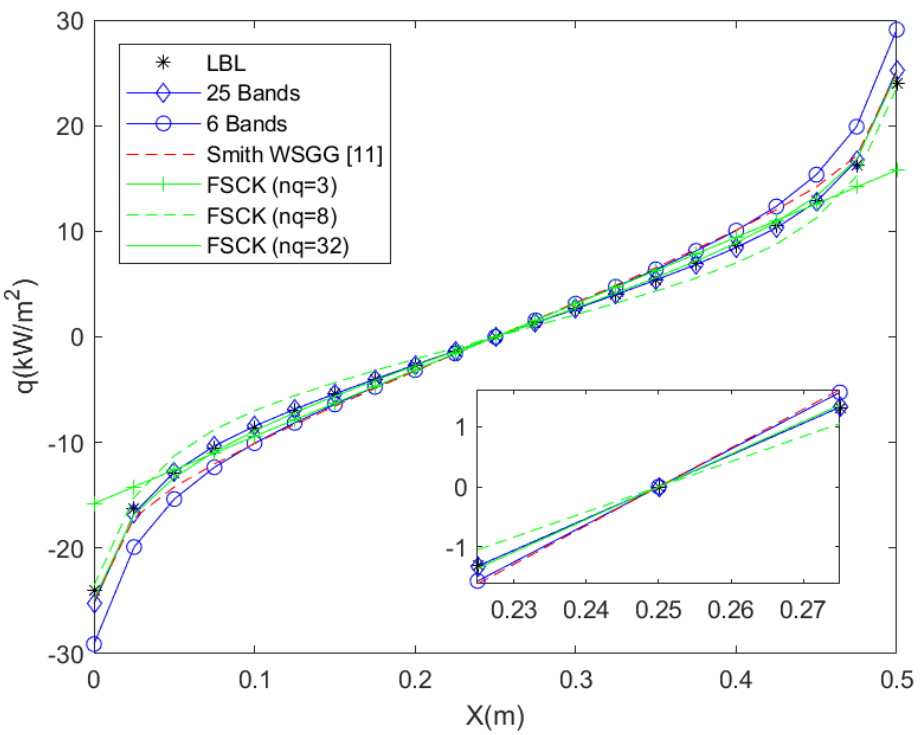

Figure 7. Radiative heat flux and radiative source along the slab for Case 3; CO_2; $\chi_{CO_2} = 0.1$, $L = 0.5\ m$, and $T = 1500K$ with black walls.

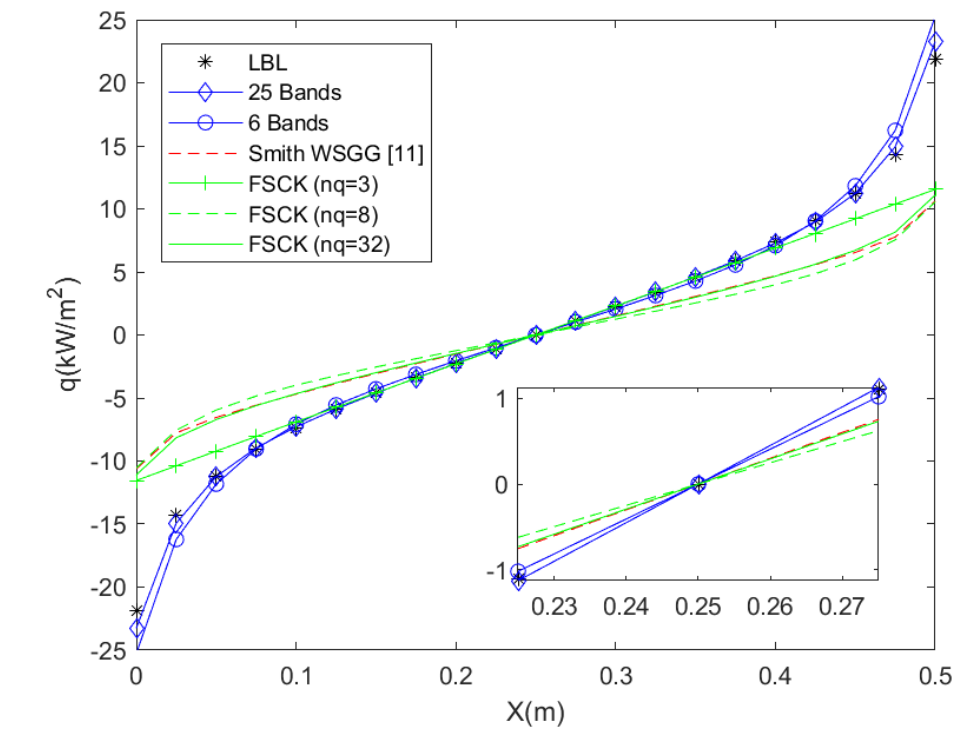

Figure 8. Radiative heat flux and radiative source along the slab for Case 4; CO_2; $\chi_{CO_2} = 0.1$, $L = 0.5\ m$, and $T = 1500K$ with non-gray walls as defined by Eq. (27).

Table 3 shows the mean values of the relative error for two different band selections together with the those of WSGG and FSCK (nq=32) of the cases defined in Table 1. In all the cases, the option of using 25 bands led to the most accurate results. Please note that the large error values reported for WSGG and FSCK in cases 2 and 4 are basically due to the fact that those models cannot support the non-grayness in the walls and their predictions have been obtained by using an average value for the gray wall emittance. Yet, results of the cases 1 and 3 show that the present banded approach provides quite accurate results with a joyful simplicity and low computational cost. It makes the method suitable for practical CFD modeling of combustion systems where too many physical phenomena need to be included and improvement of computational speed of all the sub-models are essentially important.

Looking at the results, one may notice that all the models show better accuracy in the middle of medium while have difficulties in predicting the rapid changes close to walls. It is due to rapid temperature change from the wall to the medium and therefore different Planck emissive powers. The present method also provides less accurate but still fairly good results close to the walls compared to the central regions of the medium.

Case No.	25 bands	6 bands	Smith WSGG [11]	FSCK (nq=32)
1	1.45	3.7	17.2	5.36
2	1.64	4.03	34.24	34.96
3	1.44	17.97	15.19	3.17
4	1.61	7.22	36.10	36.27

Table 3. The average of the relative error (%) of the predicted radiative heat flux in four cases of Table 1.

For pure CO_2, most of the strong absorption lines are located in certain regions of the spectrum and therefore, even using six bands led to a good level of accuracy, however, the best accuracy(<2%) can be achived by using 25 bands as reported in Table 3.

3.3. Band Selection for H_2O

In the similar way as CO_2 to identify the suitable bands for pure H_2O, the smoothed profile of LBL pressure based spectral absorption coefficient multiplied by the spectral Planck emissive intensity ($\kappa_{P,\eta} I_{b,\eta}$) at T=2400K has been used. Several values for the onsets and the thresholds of the $\kappa_{P,\eta} I_{b,\eta}$ values of the bands have been examined in three benchmarks. The benchmarks are introduced in Table 4.

Case No.	$L(m)$	χ_{H_2O}	$T(K)$	Wall emittance
5	1.0	1.0	1000	1 (black wall)
6	1.0	1.0	1000	Eq. 27 (non-gray wall)
7	2.0	0.2	1500	Eq. 27 (non-gray wall)

Table 4. Test cases of pure H_2O.

Form several examined band schemes, we show results of two best ones here as introduced in Table 5.

Thresholds of $\kappa_{P,\eta} I_{b,\eta}$	Min. value of $\kappa_{P,\eta} I_{b,\eta}$	Number of bands
$1e^{-5}$-$1e^{-4}$, $1e^{-4}$-$1e^{-3}$, $1e^{-3}$-$1e^{-2}$, $1e^{-2}$-$1e^{-1}$, 0.1-1.0	$1e^{-5}$	21
1e-4-0.006, 0.006-0.02, 0.02-1.0	$1e^{-4}$	13

Table 5. Two forms of band selection examined for pure H_2O benchmarks.

21 bands' limits(cm^{-1}): 150.00-652.6, 652.6-1160, 1160-1438, 1438-1494, 1494-1533, 1533-1551, 1551-1952, 1952-2299, 2299-2508, 2710-2908,2908-3321, 3321-3721, 3721-3745, 3745-3955, 3955-4048, 4048-4230, 4855-5043, 5043-5172, 5172-5279, 5279-5348, 5348-5639.

13 bands' limits (cm^{-1}): 150-351.7, 351.7-869.9, 869.9-1098, 1098-1511, 1511-1604, 1604-1923, 1923-2413, 2651-3033, 3033-3290, 3290-3675, 3675-4052, 4052-4210, 4603-5698.

The band divisions corresponded to the options of Table 5 are shown in Figure 9 with the thermal conditions of Case 5 of Table 4.

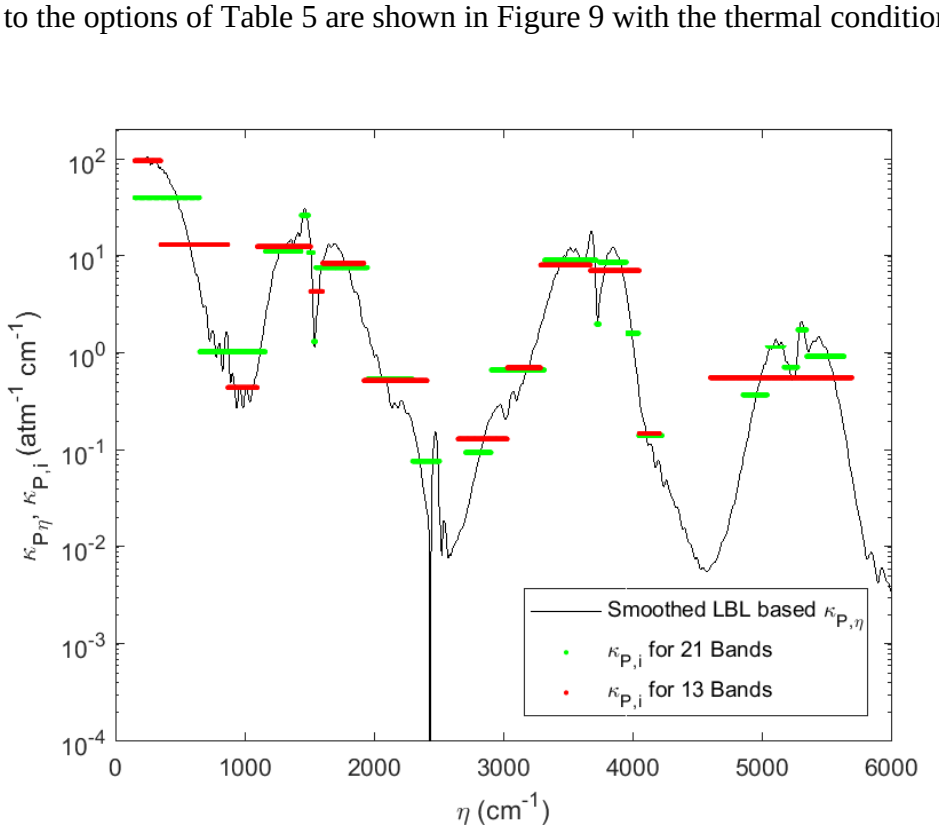

Figure 9. Illustration of how gray bands are identified for pure H_2O from the smoothed profile of the LBL pressure based spectral absorption coefficient. The figure shows the values of Case 5 of Table 4.

In Figures 10-13, the prediction of the present approach for case 5-7 of Table 4 have been compared with those of LBL reference solution, and two other methods of WSGG and FSCK. Again it should be noted that the results of global models, i.e. WSGG and FSCK, for the cases with non-gray walls, i.e. Cases 6 and 7, have been obtained by modeling the walls as gray with an average value for emittance of non-gray emittance profile (Eq. 27).

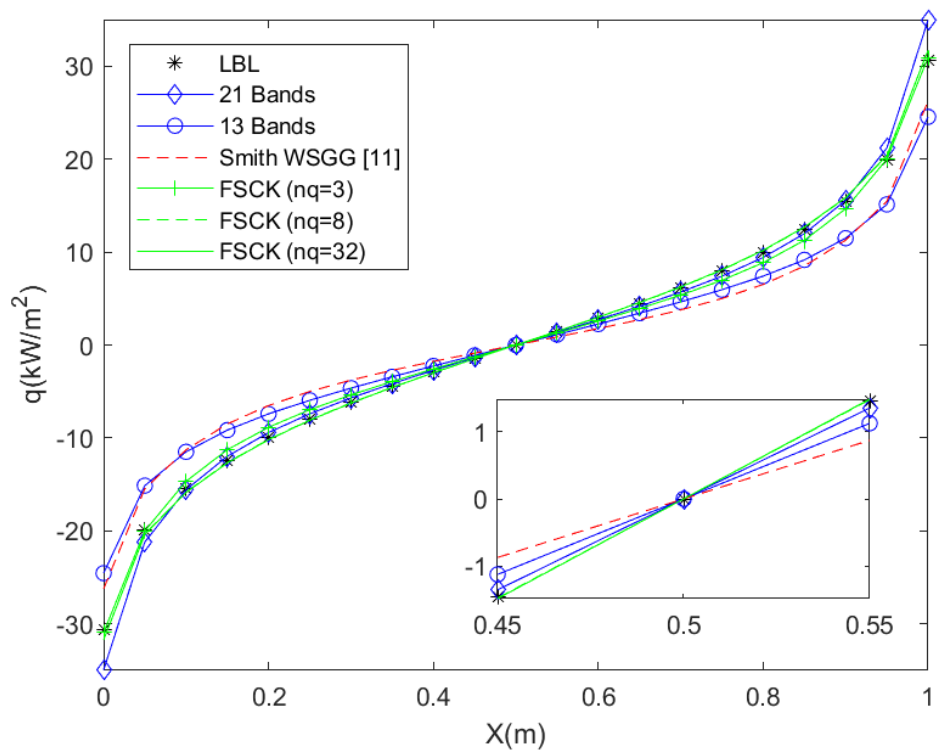

Figure 10. Radiative heat flux and radiative source along the slab for Case 5; H_2O; $\chi_{H_2O}=1.0$, $L=1.0\ m$, and $T=1000K$ with black walls.

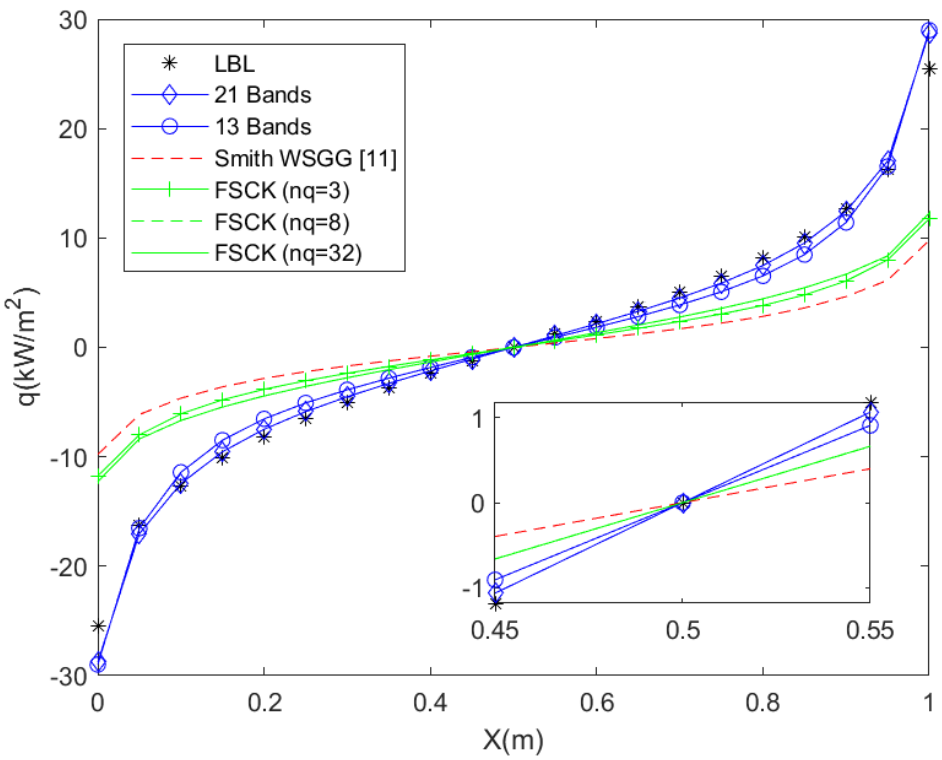

Figure 11. Radiative heat flux and radiative source along the slab for Case 6; H_2O; $\chi_{H_2O}=1.0$, $L=1.0\ m$, and $T=1000K$ with non-gray walls as defined by Eq. (27).

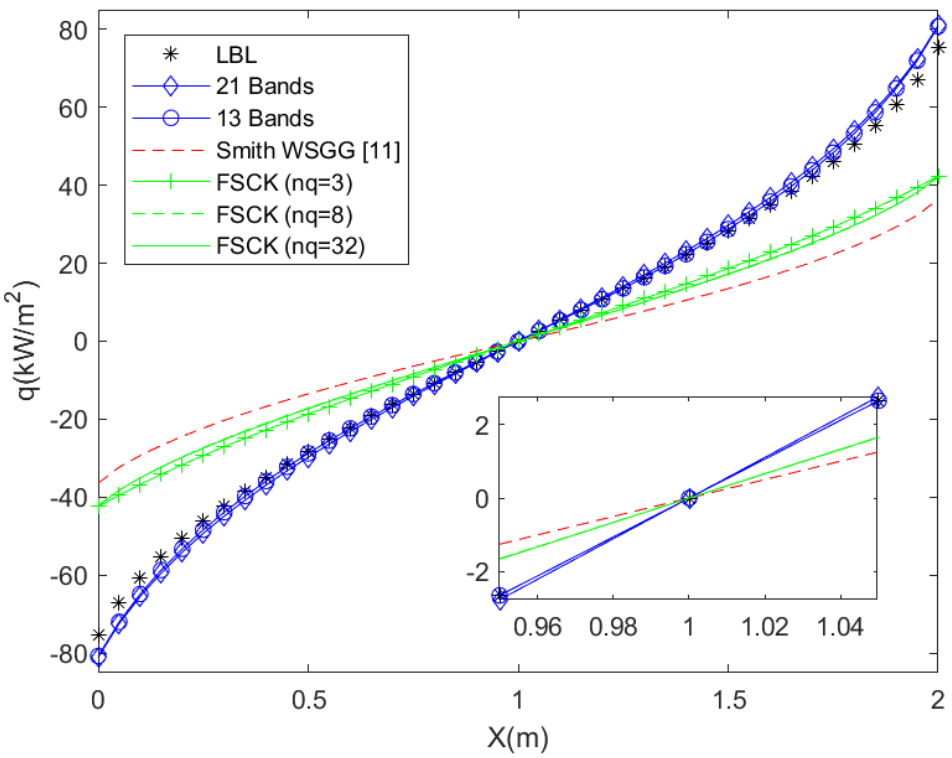

Figure 12. Radiative heat flux and radiative source along the slab for Case 7; H_2O; $\chi_{H_2O} = 0.2$, $L = 2.0\ m$, and $T = 1500K$ with non-gray walls as defined by Eq. (27).

Case 7 has a larger optical thickness compared to case 5 and 6. It causes better performance for the present approach as seen in Figure 12. The accuracy is good even in the regions close to walls. It is because of the fact that larger optical thickness improves the correctness of assuming constant absorption coefficient within the bands. Expectedly, the method exhibits less accuracy in the cases with smaller optical thickness such as Case 5 as shown in Figure 10 especially in the close to wall regions.

The average of the relative error of radiative heat flux calculated by different models for the cases of pure H_2O (Table 4) are mentioned in table 6.

Case No.	21 bands	13 bands	Smith WSGG [11]	FSCK (nq=32)
5	6.34	23.00	31.02	2.02
6	7.91	15.38	17.30	43.90
7	3.65	5.49	14.77	38.61

Table 6. The average of the relative error (%) of the predicted radiative heat flux in the cases of pure H_2O (Table 4).

Compared to CO_2, for H_2O, the absorption lines are more distributed along the spectrum and therefore more bands are needed. The division scheme with 21 bands presented in Table 5 showed a good level of accuracy (<8%) for all the cases of pure H_2O.

3.4. Band Selection for CO_2-H_2O Mixture

In the similar way as pure H_2O and pure CO_2, for the cases in which both gases exist, the smoothed profiles of LBL pressure based spectral absorption coefficient of each individual gas at T=2400K have been used for identifying the bands. To obtain the smoothed histogram for this case, in each spectral location the LBL spectral absorption coefficient of individual gases have been summed up. Figure 13 shows the smoothed profile of spectral absorption coefficient with the gray band absorption coefficient of two options of the band selections as introduced in Table 7 for the thermal conditions corresponded to case 8. The selected bands have been examined in some benchmarks as shown in Table 8.

Thresholds of $\kappa_{P,\eta} I_{b,\eta}$	Min. value of $\kappa_{P,\eta} I_{b,\eta}$	Number of bands
$1e^{-3}$-$1e^{-2}$, $1e^{-2}$-$1e^{-1}$, $1e^{-1}$-1.0	$1e^{-3}$	15
$1e^{-4}$-0.006, 0.006-0.01, 0.01-$1e^{-1}$, $1e^{-1}$-1.0	$1e^{-4}$	31

Table 7. Two forms of band selection examined for the mixture of H_2O-CO_2 benchmarks.

15 bands' limits(cm^{-1}): 175.7-445.1, 445.1-764, 764-1163, 1163-1497, 1497-1996, 1996-2065, 2065-2341, 2341-2358, 2358-2494, 2651-3124, 3124-4011, 4011-4210, 4529-5698, 6477-7192, 7229-7472.

31 bands' limits (cm^{-1}): 150-351.6, 351.6-555, 555-712, 712-866.7, 866,7-1104, 1104-1163, 1163-1497, 1497-1604, 1604-1850, 1850-1996, 1996-2065, 2065-2341, 2341-2358, 2358-2362, 2362-2496, 2496-2659, 2659-3124, 3124-3335, 3335-3697, 3697-3809, 3809-4011, 4011-4210, 4210-4531, 4531-5076, 5076-5277, 5277-5698, 5698-6477, 6477-7136, 7136-7400, 7400-7418, 7418-7472.

The band selection schemes for the case of H_2O-CO_2 mixture have been tested in three benchmarks as presented in Table 8. Case 8 and 9 represent the typical air and oxy-fired gas compositions, respectively with a uniform temperature while temperature and gas compositions in Case 10 are inhomogeneous.

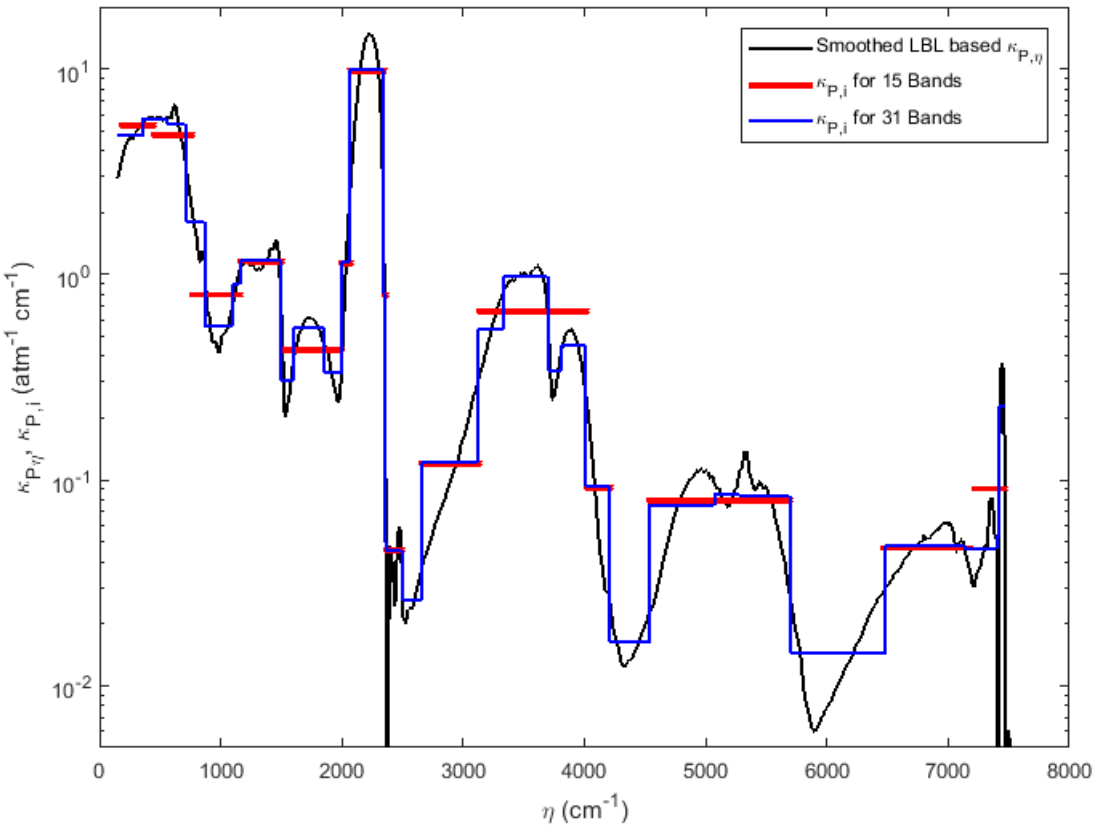

Figure 13. Illustration of how gray bands are identified for mixture of H_2O and CO_2 from smoothed profile of the LBL spectral pressure based absorption coefficient. The figure shows the values of Case 8 of Table 7.

Case No.	$L(m)$	χ_{H_2O}	χ_{CO_2}	$T(K)$	Wall emittance
8	1.0	0.2	0.1	2400	1 (black wall)
9	1.0	0.15	0.85	1500	Eq. 27 (non-gray wall)
10	1.0	See Fig. 16	See Fig. 16	See Fig. 16	Eq. 27 (non-gray wall)

Table 8. Test cases of the mixture of H_2O and CO_2.

Figures 14 and 15 show the results of the present model for the Cases 8 and 9 of Table 8.

Table 9 shows the error associated with three different band selection schemes for three cases of Table 8.

Case No.	31 bands	15 bands	Bordbar WSGG [4]	FSCK (nq=32)
8	0.85	2.98	28.78	28.27
9	8.35	11.42	45.92	39.98

Table 9. The average of the relative error (%) of the predicted radiative heat flux in the first two cases of H_2O-CO_2 mixture (Table 8).

Comparing Figures 14 and 15 and also the results presented in Table 1, it is seen that the results of the present approach for the case 8 is more accurate than case 9. It is explained by the fact that temperature of case 8 is the same as the temperature in which the smoothed histogram for selection of band limits has been obtained. In other words, the present approach shows better performance when the temperature of the medium is closer to 2400K in which the band limits have been determined from the LBL based smoothed histogram of spectral absorption coefficient. In fact the obtained bands from the histogram at 2400 K might be larger than the real active bands at very low temperatures and it is expected to enhance inaccuracy to the model as can be seen by comparison between case 8 and 9.

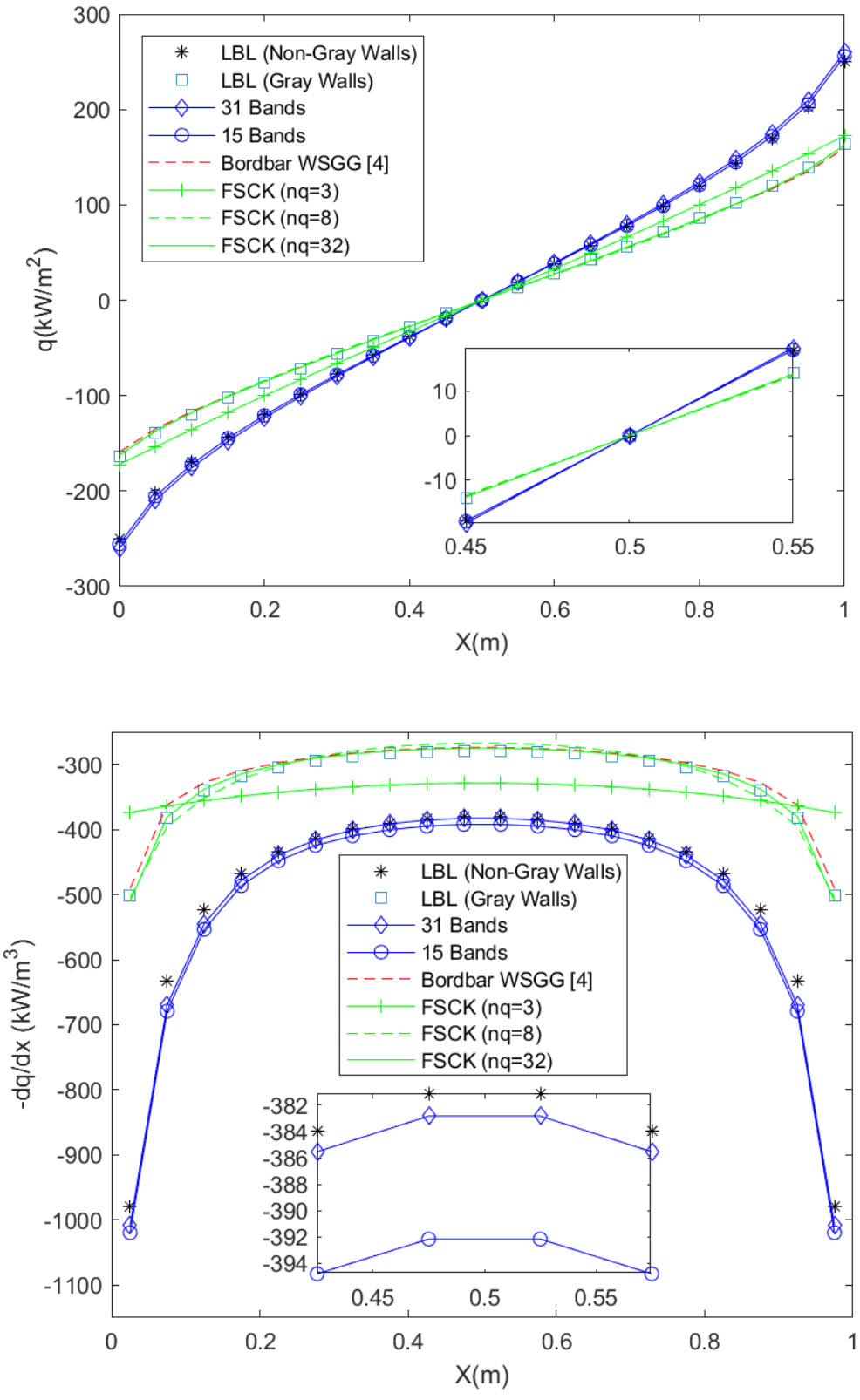

Figure 14. Radiative heat flux and radiative source along the slab for Case 8; Homogeneous H_2O-CO_2 Mixture; $\chi_{H_2O} = 0.2, \chi_{CO_2} = 0.1, , L = 1.0\ m$, and $T = 2400K$ with non-gray walls as defined by Eq. (27).

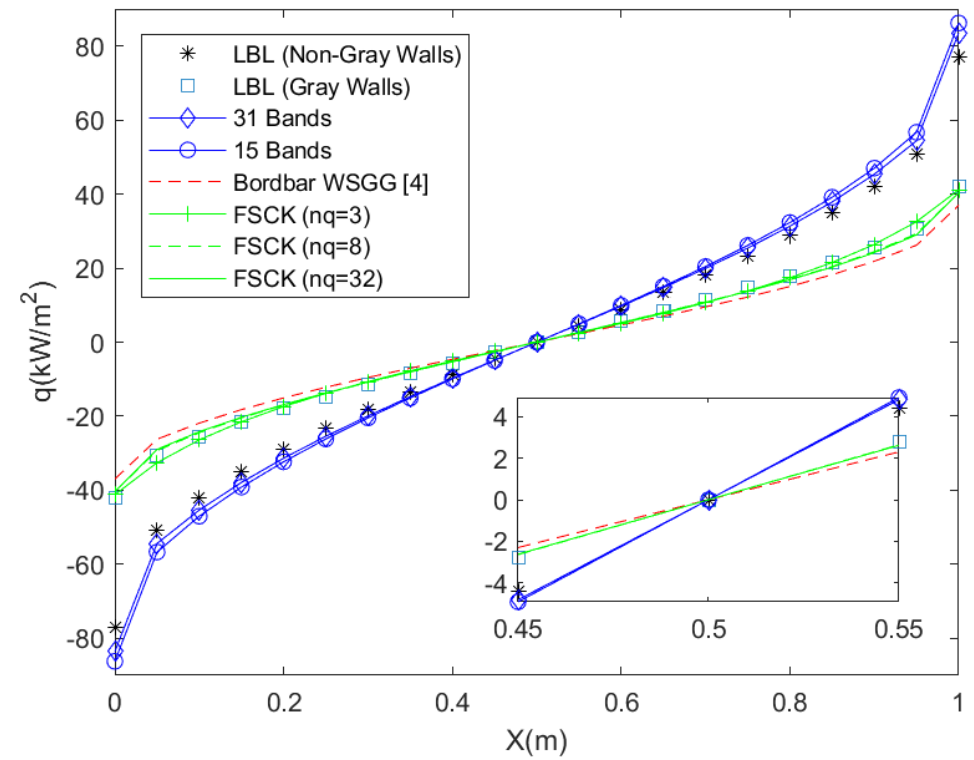

Figure 15. Radiative heat flux and radiative source along the slab for Case 9; Homogeneous H_2O-CO_2 Mixture; $\chi_{H_2O} = 0.15, \chi_{CO_2} = 0.85, , L = 1.0\ m$, and $T = 1500K$ with non-gray walls as defined by Eq. (27).

3.5. Correlations for Band Absorption Coefficients

To make the present method simple to be used for radiation heat transfer modeling in a general combustion systems, some polynomial correlations have been obtained for pressure based gray band absorption coefficients of pure H_2O and pure CO_2. Analyzing the results of Case 1 to Case 9, we have selected the band divisions with 31 bands, as described in Table 7 and shown in Figure 13, as our final choice to be used for obtaining the general correlations of gray band absorption coefficient. This scheme provides better accuracy in all the test cases. It was found that use of finer resolution for selection of gray bands had negligible influence on the results but increase the computation time significantly.

To obtain the correlations, for each gas, the database of gray band absorption coefficients of 31 bands have been obtained from LBL data by using Eq. (15). For the temperatures of 300 to 2400 K with the step of 50 K, the databases of pressure based gray band absorption coefficients have been obtained. A sixth order polynomial function was then implemented to approximate the gray band absorption coefficient of each gas in each band as the function of temperature as

$$\bar{\kappa}_{P,i}\Big|_{i=1\,to\,31} = \sum_{j=0}^{6} b_{i,j} T^{(6-j)} \tag{28}$$

The least square method has been used to find the coefficients of the correlations. The obtained coefficients have been reported in the Appendix I. Note that the gray band absorption coefficient of the mixture is the sum of the gray band absorption coefficients of the individual gases including the effect of mole fractions as explained by Eq. (26).

To validate the correlations, they have been used to model Case 10 of Table 8 that represent inhomogeneous media. The profiles of temperature, CO_2 and H_2O mole fractions for Case 10 are shown in Figure 16. Figure 17 shows the results of implementing two different band dividing schemes as shown in Table 7 and Figure 13 in modeling of Case 10. The relative error of the predicted radiative heat flux for 31 bands is 4.72 %.

Defining different test cases was done in the way that in each of three situations, i.e. pure CO_2, pure H_2O and mixture of H_2O-CO_2, the band selections were examined at least in two different thermal conditions and optical thicknesses in each of three scenarios, see Tables 1, 4, and 8. However, the model is expected to provide different level of accuracy in different conditions. In fact, all the simplified non-gray models provide various level of accuracy in different thermal and optical conditions and the present model is not an exception. Yet, it should be noted that the present approach provides a practical and simple way to support non-grayness of the walls which is not possible with the global models as they are based on reordering of wavenumbers. Moreover, comparing to other available models, the calculation procedure of the present approach is much simpler consisting of calculation of some polynomial functions for the band gray absorption coefficient and the blackbody fractional function of the bands as the weighting factors.

4. Summary and Conclusions

By analyzing the line by line based profile of the pressure based spectral absorption coefficient of CO_2 and H_2O in different thermodynamic states, several band dividing schemes have been selected and tested in ten different one-dimensional benchmarks representing pure CO_2, pure H_2O and mixture of these two main combustion gases in typical air and oxygen fired conditions.

As the line by line spectral profiles include large local variation, an smoothing technique has been implemented to make a simpler profile of $\kappa_{P,\eta} I_{b,\eta}$ at the highest temperature in our range of interest (2400K). The smoothed profiles allowed us to identify the wave number of different thershold values which was set for different dividing schemes.

Compared to the global models, in the present approach, the wavenumbers are not reordered, and therefore the information of the spectral location corresponded to each gray absorption coefficients is known. Hence, the present model can support spectrally dependent radiation properties on the walls, i.e., non-gray walls. In addition, this method supports the applications when the spectral radiative heat transfer is important such as fire sensors.

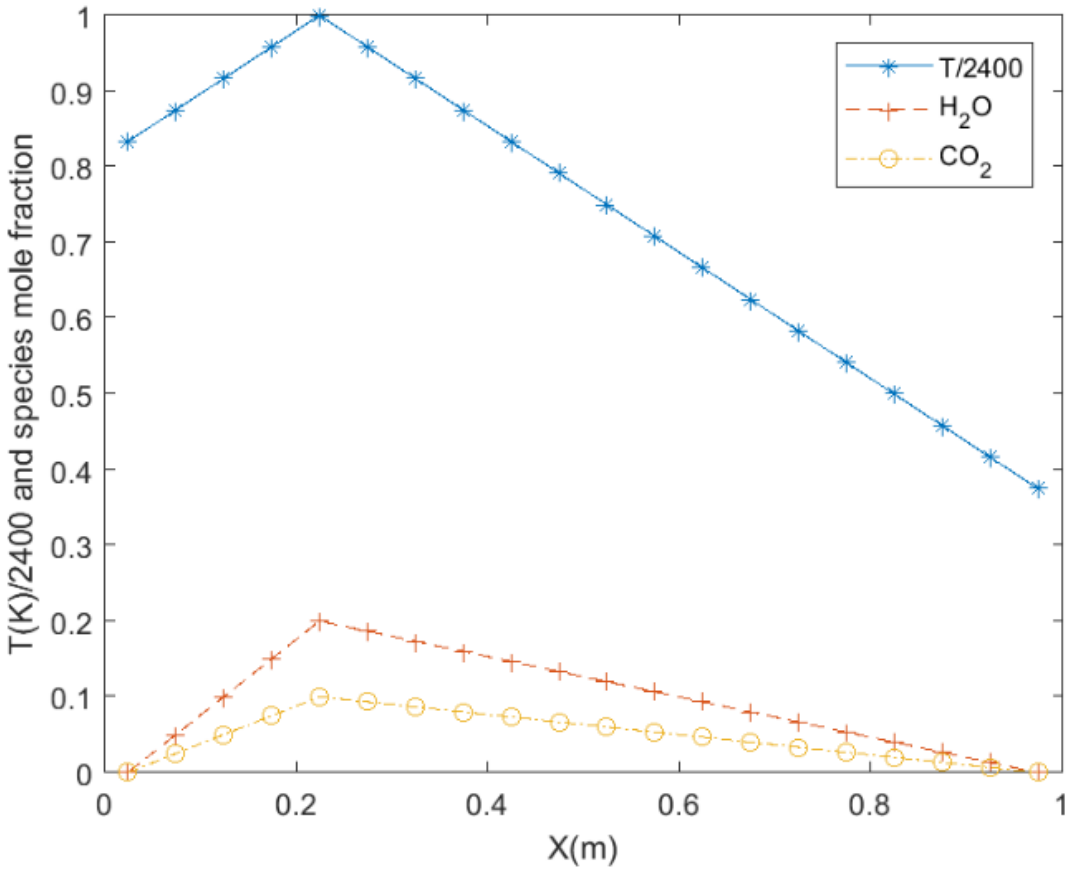

Figure 16. Temperature, CO_2, and H_2O mole fraction distributions for Case 10 of Table 8.

Several dividing scheme have been assessed for the cases of gas mixture. The division scheme with 31 bands have been selected to obtain the general correlations for gray band absorption coefficients. This scheme is chosen because it provides best accuracy compared with the other options in all the cases. In this paper the base of the scheme selection was on accuracy. It can be further improved in next papers by optimizing the CPU cost as well as accuracy.

Using the LBL based datasets for the pressure based spectral absorption coefficient at various temperatures, a series of polynomial function of temperature has been determined to provide a simple way for calculating the pressure based gray band absorption coefficient in the selected 31 bands. The obtained correlations have been validated in the case of inhomogeneous media (Case 10).

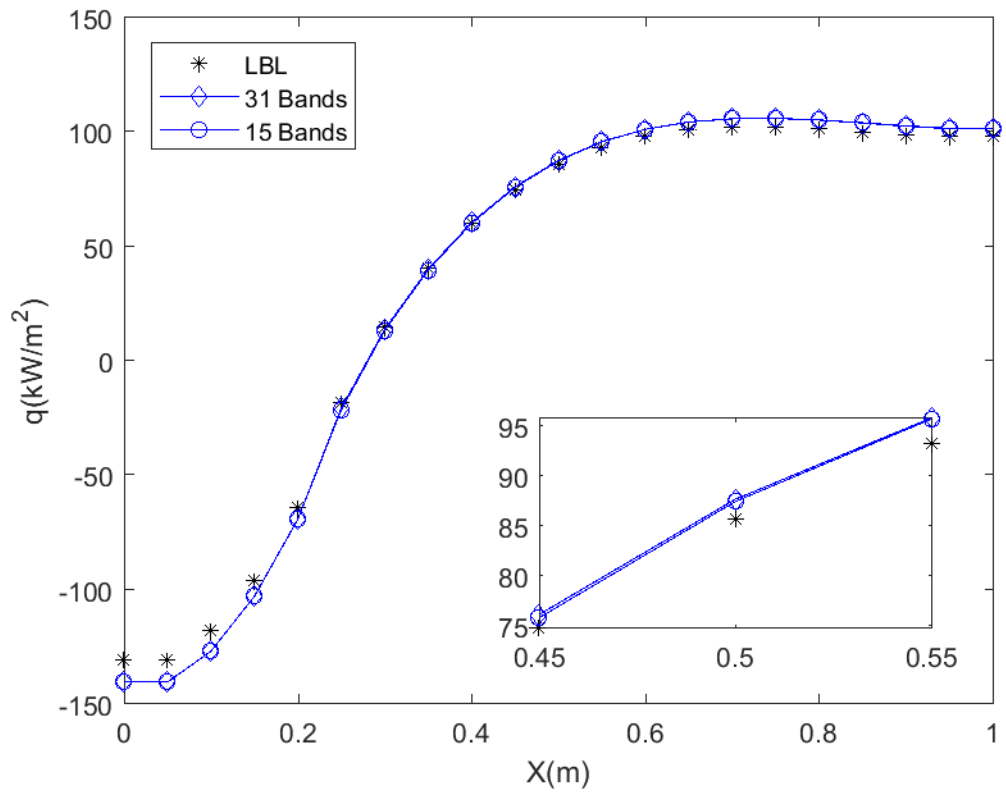

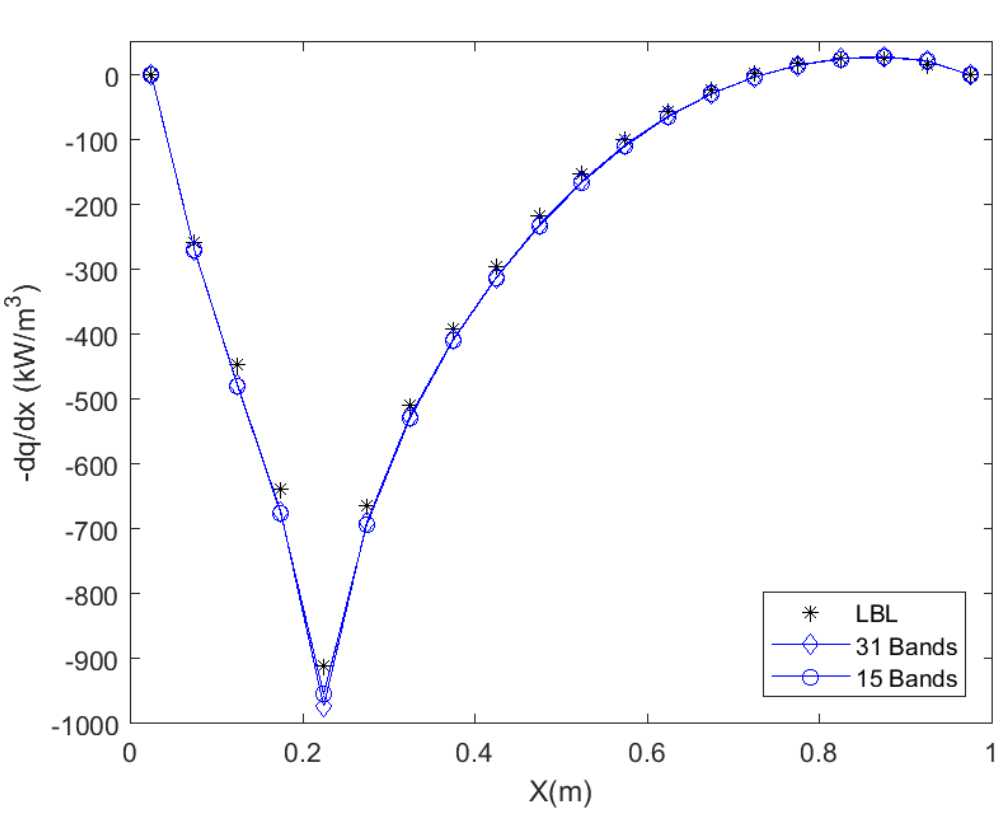

Figure 17. Radiative heat flux and radiative source along the slab for Case 10; inhomogeneous H_2O-CO_2 mixture; the distributions of gas species and temperature are shown in Figure 14 with non-gray walls as defined by Eq. (27).

5. Acknowledgments

This work was conducted out within the project Clustering Innovation Competence of Future Fuels in Power Production (CLIFF, 2014-2017) as part of the activities of the “Lappeenranta University of Technology”. Other research partners are Åbo Akademi University, VTT Technical Research Centre of Finland, Ltd., Aalto University, and Tampere University of Technology. Support from the National Technology Agency of Finland (Tekes), Andritz Oy, Valmet Technologies Oy, Amec Foster Wheeler Energia Oy, UPM-Kymmene Oyj, Clyde Bergemann GmbH, International Paper, Inc., and Top Analytica Oy Ab is gratefully acknowledged.

Authors would like to thank Professor M. Modest from University of California-Merced for providing the look up tables used in obtaining the parameters of FSCK model.

References

[1] M. Modest, Radiative Heat Transfer, Third ed., New York: Elsevier, 2013.

[2] M. H. Bordbar, K. Myöhänen and T. Hyppänen, "Coupling of a radiative heat transfer model and a three-dimensional combustion model for a circulating fluidized bed furnace," *Applied Thermal Engineering,* vol. 76, p. 344–356, 2015.

[3] M. H. Bordbar and T. Hyppänen, "The correlation based zonal method and its application to the back pass channel of oxy/air-fired CFB boiler," *Applied Thermal Engineering,* vol. 78, p. 351–363, 2015.

[4] M. H. Bordbar, G. Wecel and T. Hyppänen, "A line by line based weighted sum of gray gases model for inhomogeneous CO2–H2O mixture in oxy-fired combustion," *Combustion and Flame,* vol. 161, no. 9, p. 2435–2445, 2014.

[5] H. Chu, F. Liu and H. Zhou, "Calculations of gas thermal radiation transfer in one-dimensional planar enclosure using LBL and SNB models," *International Journal of Heat and mass transfer,* vol. 54, p. 4736–4745., 2011.

[6] R. Goody, "A statistical model for water vapour absorption," *Quart. J. R. Meteorol. Soc. ,* vol. 78, pp. 165-169, 1952.

[7] A. Soufiani and J. Taine, "High Temperature Gas Radiative Property Parameters of Statistical Narrow-band Model for H2o, Co2 and Co, and Correlated-k Model for H2o and Co2," *International Journal of Heat and Mass Transfer,* vol. 40, pp. 987-991, 1997.

[8] P. Rivière and A. Soufiani, "Updated band model parameters for H 2O, CO 2, CH 4 and CO radiation at high temperature," *International Journal of Heat and Mass Transfer,* vol. 55, no. 13-14, p. 3349–3358, 2012.

[9] D. Edwards, "Molecular Gas Band Radiation," *Advances in Heat Transfer,* vol. 12, p. 115–193, 1976.

[10] H. C. Hottel and A. F. Sarofim, Radiative Transfer, New York: McGraw-Hill Education, 1967.

[11] T. Smith, Z. Shen and J. Friedman, "Evaluation of Coefficients for the Weighted Sum of Gray Gases Model," *Journal of Heat Transfer,* vol. 104, no. 4, pp. 602-608, 1982.

[12] M. F. Modest and H. Zhang, "The Full-Spectrum Correlated-k Distribution for Thermal Radiation From Molecular Gas-Particulate Mixtures," *Journal of Heat Transfer,* vol. 124, pp. 30-38, 2002.

[13] C. Wang, W. Ge, M. F. Modest and B. He, "A full-spectrum k-distribution look-up table for radiative transfer in nonhomogeneous gaseous media," *Journal of Quantitative Spectroscopy and Radiative Transfer,* vol. 168, pp. 46-56, 2016.

[14] M. K. Denison and B. W. Webb, "A Spectral Line-Based Weighted-Sum-of-Gray-Gases Model for Arbitrary RTE Solvers," *Journal of Heat Transfer,* vol. 115, no. 4, pp. 1004-1012, 1993.

[15] V. P. Solovjov, F. Andre, D. Lemonnier and B. W. Webb, "The Generalized SLW Model," *Journal of Physics: Conference Series,* vol. 676, p. 012022, 2016.

[16] P. Rivière, A. Soufiani, M.-Y. Perrin, H. Riad and A. Gleizes, "Air mixture radiative property modelling in the temperature range 10,000–40,000 K," *Journal of Quantitative Spectroscopy and Radiative Transfer,* vol. 56, no. 1, pp. 29-45, 1996.

[17] M. F. Modest and R. J. Riazzi, "Assembly of full-spectrum k-distributions from a narrow-band database; effects of mixing gases, gases and nongray absorbing particles, and mixtures with nongray scatterers in nongray enclosures," *Journal of Quantitative Spectroscopy and Radiative Transfer,* vol. 90, no. 2, pp. 169-189, 2005.

[18] A. G. Clements, R. Porter, A. Pranzitelli and M. Pourkashanian, "Evaluation of FSK models for radiative heat transfer under oxyfuel conditions," *Journal of Quantitative Spectroscopy and Radiative Transfer,* vol. 151, pp. 67-75, 2015.

[19] L. Rothman, I. Gordon, Y. Babikov, A. Barbe, . D. Chris Benner, . P. Bernath, M. Birk, L. Bizzocchi, V. Boudon and et al., "The HITRAN2012 molecular spectroscopic database," *Journal of Quantitative Spectroscopy and Radiative Transfer,* vol. 130, p. 4–50, 2013.

[20] C. Wang, M. F. Modest and B. He, "Improvement of full-spectrum k-distribution method using quadrature transformation," *International Journal of Thermal Sciences,* vol. 108, pp. 100-107, 2016.

[21] F. Liu, H. A. Becker and A. Pollard, "Spatial differencing schemes of the discreteordinates," *Numerical Heat Transfer B,* vol. 30, pp. 23-43, 1996.

[22] L. S. Rothman, I. E. Gordon, R. J. Barber, H. Dothe, R. R. Gamache, . A. Goldman, V. I. Perevalov, S. A. Tashkun and J. Tennyson, "HITEMP, the high-temperature molecular spectroscopic database," *Journal of Quantitative Spectroscopy and Radiative Transfer,* vol. 111, pp. 2139-2150, 2010.

[23] "MATLAB online help," [Online]. Available: https://se.mathworks.com/help/curvefit/smoothing-data.html.

320

325

Appendix I: Tables of the coefficients for the correlations of the pressure based gray band absorption coefficients of CO_2 and H_2O.

Table A.1*: Coefficients for the correlations of the pressure based gray band absorption coefficient ($m^{-1}. atm^{-1}$) for pure H_2O at atmospheric pressure.

Band No. (i)	Band Limits (cm^{-1})	$b_{i,0}$ $\times 10^{20}$	$b_{i,1}$ $\times 10^{17}$	$b_{i,2}$ $\times 10^{12}$	$b_{i,3}$ $\times 10^{8}$	$b_{i,4}$ $\times 10^{4}$	$b_{i,5}$ $\times 10^{2}$	$b_{i,6}$ $\times 10$
1	*150-351.6*	-3116.809	28246.58	-1020.932	184.569	-16.568	50.776	1694.838
2	*351.6-555*	1358.922	-12072.86	420.809	-70.96	5.511	-12.111	89.408
3	*555-712*	-290.301	2592.489	-88.562	14.000	-0.983	3.509	-44.643
4	*712-866.7*	37.857	-328.578	10.855	-1.752	0.163	-0.631	8.96
5	*8667-1104*	-12.902	114.698	-3.909	0.616	-0.038	0.11	-0.78
6	*1104-1163*	-42.214	369.576	-12.311	1.848	-0.111	0.328	-2.785
7	*1163-1497*	-348.078	3100.598	-110.389	19.853	-1.833	6.711	147.346
8	*1497-1604*	2537.687	-23106.540	851.226	-162.507	17.049	-94.771	2288.787
9	*1604-1850*	1277.706	-11654.990	430.618	-82.659	8.780	-50.537	1374.642
10	*1850-1996*	-63.611	546.488	-18.522	3.131	-0.275	1.121	9.907
11	*1996-2065*	-0.57	20.446	-1.469	0.455	-0.072	0.56	-9.27
12	*2065-2341*	6.947	-63.901	2.342	-0.426	0.038	-0.11	1.23
13	*2341-2358*	-4.88	40.749	-1.274	0.176	-0.009	0.013	0.164
14	*2358-2362*	-2.392	22.697	-0.825	0.139	-0.01	0.029	-0.18
15	*2362-2496*	-3.33	27.11	-0.821	0.108	-0.005	0.001	0.275
16	*2496-2659*	0.603	-5.398	0.188	-0.032	0.003	-0.018	0.438
17	*2659-3124*	-0.172	0.865	-0.023	0.001	0.002	-0.016	1.493
18	*3124-3335*	-9.537	79.452	-2.198	0.146	0.025	-0.21	9.085
19	*3335-3697*	-216.254	1913.582	-67.437	11.911	-1.054	3.17	145.609
20	*3697-3809*	2690.634	-24472.92	900.064	-171.371	17.899	-98.758	2357.223
21	*3809-4011*	22.888	-294.92	15.377	-4.247	0.681	-6.504	342.373
22	*4011-4210*	-6.392	52.296	-1.587	0.208	-0.01	0.015	1.265
23	*4210-4531*	0.69	-6.439	0.241	-0.045	0.004	-0.019	0.382
24	*4531-5076*	2.62	-24.36	0.913	-0.174	0.017	-0.053	0.618
25	*5076-5277*	18.736	-187.228	7.777	-1.743	0.228	-1.738	68.624
26	*5277-5698*	189.574	-1719.278	62.998	-11.938	1.24	-6.829	169.872

27	*5698-6477*	0.00689	-0.00797	-0.00426	0.00171	0.00004	-0.00067	0.0747
28	*6477-7136*	-6.789	62.988	-2.366	0.459	-0.048	0.254	-1.576
29	*7136-7400*	118.614	-1082.151	40.007	-7.69	0.819	-4.724	127.688
30	*7400-7418*	26.724	-239.883	8.489	-1.471	0.123	-0.382	4.816
31	*7418-7472*	-46.671	383.061	-11.757	1.605	-0.088	0.183	-0.169

*Higher precision coefficients can be obtained by contacting the first author.

Table A.2*: Coefficients for the correlations of the pressure based gray band absorption coefficient for pure CO_2 at atmospheric pressure.

Band No. (i)	Band Limits (cm^{-1})	$b_{i,0}$ $\times 10^{20}$	$b_{i,1}$ $\times 10^{17}$	$b_{i,2}$ $\times 10^{12}$	$b_{i,3}$ $\times 10^{8}$	$b_{i,4}$ $\times 10^{4}$	$b_{i,5}$ $\times 10^{2}$	$b_{i,6}$ $\times 10$
1	*150-351.6*	0.315043	-2.822	0.102	-0.019	0.002	-0.011	0.281
2	*351.6-555*	16.654	-127.239	3.456	-0.317	-0.025	0.655	-12.998
3	*555-712*	2970.11	-27227.68	1013.409	-196.781	21.298	-126.760	3736.652
4	*712-866.7*	23.029	-210.581	7.766	-1.46	0.139	-0.481	5.87
5	*8667-1104*	11.094	-96.337	3.298	-0.556	0.045	-0.108	0.713
6	*1104-1163*	0.357	-3.234	0.118	-0.022	0.002	-0.013	0.302
7	*1163-1497*	0.396	-3.593	0.132	-0.025	0.003	-0.015	0.358
8	*1497-1604*	0.580	-5.256	0.193	-0.037	0.004	-0.021	0.519
9	*1604-1850*	0.976	-8.741	0.316	-0.059	0.006	-0.033	0.818
10	*1850-1996*	2.469	-23.019	0.843	-0.155	0.016	-0.085	2.202
11	*1996-2065*	48.089	-545.2	21.501	-3.72	0.316	-1.287	21.959
12	*2065-2341*	667.07	-8248.341	423.586	-117.595	19.158	-186.405	10326.54
13	*2341-2358*	1444.158	-13826.88	526.763	-99.871	9.483	-38.935	591.792
14	*2358-2362*	93.862	-853.174	31.37	-5.978	0.627	-3.502	86.076
15	*2362-2496*	32.461	-293.978	10.751	-2.031	0.21	-1.145	26.99
16	*2496-2659*	5.091	-46.144	1.69	-0.32	0.033	-0.181	4.283
17	*2659-3124*	1.601	-14.461	0.527	-0.099	0.01	-0.055	1.265
18	*3124-3335*	9.878	-78.409	2.285	-0.301	0.02	-0.067	0.965
19	*3335-3697*	-38.252	281.539	-6.682	0.182	0.161	-2.566	177.407
20	*3697-3809*	49.276	-389.89	11.294	-1.312	0.013	0.741	-17.458
21	*3809-4011*	0.316	-2.913	0.11	-0.021	0.002	-0.012	0.269
22	*4011-4210*	0.147	-1.333	0.049	-0.009	0.001	-0.005	0.125
23	*4210-4531*	0.252	-2.039	0.063	-0.01	0.001	-0.004	0.089
24	*4531-5076*	-1.339	11.645	-0.391	0.061	-0.004	0.003	1.423
25	*5076-5277*	-0.568	5.468	-0.214	0.043	-0.005	0.026	-0.287
26	*5277-5698*	0.034	-0.311	0.012	-0.002	0.0003	-0.002	0.038
27	*5698-6477*	-0.005	0.047	-0.001	0.0001	0.00002	0.00035	0.027

28	*6477-7136*	-0.045	0.396	-0.014	0.0023	0.00018	0.00074	0.0331
29	*7136-7400*	0.015	-0.133	0.005	-0.00091	0.0001	-0.00053	0.013
30	*7400-7418*	0.019	-0.176	0.007	-0.00125	0.00013	-0.00074	0.017
31	*7418-7472*	0.016	-0.146	0.005	-0.00106	0.00011	-0.00063	0.01499

*Higher precision coefficients can be obtained by contacting the first author.

350